KLF6 Downregulation-Mediated Loss of LILRB4 Impairs Decidual Macrophage Tolerance During Toxoplasma gondii Infection

Xuemei Hu

xuemeihu@bzmc.edu.cn

Shandong Medical and Pharmaceutical University

Zhidan Li

Fan Zhang

Shandong Medical and Pharmaceutical University

Rutao Mou

Shandong Medical and Pharmaceutical University

Tianyu Jing

Shandong Medical and Pharmaceutical University

Zhendong Zhang

Shandong Medical and Pharmaceutical University

Xianbing Liu

Liqin Ren

Shandong Medical and Pharmaceutical University

Yuzhu Jiang

Haixia Zhang

Article

Keywords: T. gondii, Infection, Decidual macrophage, Abnormal pregnancy, KLF6, LILRB4, Maternal-fetal tolerance

Posted Date: July 1st, 2026

DOI: https://doi.org/10.21203/rs.3.rs-10053928/v1

Additional Declarations: There is **NO** Competing Interest.

KLF6 Downregulation-Mediated Loss of LILRB4 Impairs Decidual Macrophage Tolerance During *Toxoplasma gondii* Infection

Zhidan Li[1], Fan Zhang[1], Rutao Mou[2], Tianyu Jing[1], Zhendong Zhang[1], Xianbing Liu[1], Liqin Ren[3], Yuzhu Jiang[1], Haixia Zhang[1], Xuemei Hu[1]✉

[1]Department of Immunology, Shandong Medical and Pharmaceutical University, Yantai, Shandong, P. R. China, 264003.

[2]Yantai Mountain Hospital, Yantai, Shandong, P. R. China, 264003.

[3]Department of Pathogen Biology, Shandong Medical and Pharmaceutical University, Yantai, Shandong, P. R. China, 264003.

✉**Correspondence:**

Xuemei Hu, Department of Immunology, Shandong Medical and Pharmaceutical University, #346 Guan-hai Road, Lai-shan, Yantai, Shandong, P.R. China, 264003,

E-mail: xuemeihu@bzmc.edu.cn

Running title: *T. gondii*-mediated LILRB4 reduction disrupted dMφ

Summary

Toxoplasma gondii (*T. gondii*) infection during pregnancy can cause miscarriage and stillbirth, yet its underlying mechanisms remain unclear. The inhibitory receptor leukocyte immunoglobulin-like receptor B4 (LILRB4), highly expressed on decidual macrophages (dMφ), is essential for maintaining maternal-fetal tolerance. We have reported that *T. gondii* infection reduced LILRB4 levels on dMφ, correlating with adverse pregnancy outcomes (APOs). However, how *T. gondii* infection triggers LILRB4 reduction and consequent dysfunction in dMφ is still unclear. Here, we identified the transcription factor Krüppel-like factor 6 (KLF6) as a direct transcription factor of LILRB4, binding to the LILRB4 promoter region (-591 to -601 bp). Infection suppressed KLF6 expression and the binding ability to the promoter by inhibiting STAT3 phosphorylation, thereby reducing LILRB4 transcription and expression. LILRB4 downregulation further disrupted the immunoregulatory balance in dMφ, characterized by decreased indoleamine 2,3-dioxygenase (IDO) and increased inducible nitric oxide synthase (iNOS). Mechanistically, reduced LILRB4 expression suppressed IDO levels via the phosphorylated Src homology 2 domain-Containing Protein Tyrosine Phosphatase-1(pSHP-1)/pJAK2 (Phosphorylated Janus Kinase 2)/Phosphorylated Signal Transducer and activator of transcription 1 (Tyr701) pSTAT1 (Y701)/interferon regulatory factor 1 (IRF1) pathway while promoting iNOS expression through the pSHP-1/phosphorylated phosphatidylinositol 3-kinase (pPI3K)/cellular Fos (c-Fos) axis. Collectively, *T. gondii* infection disrupts maternal-fetal tolerance by downregulating LILRB4 expression in dMφ through the pSTAT3(705)/KLF6 axis, resulting in IDO/iNOS dysregulation and subsequent APOs. This study highlights LILRB4 as a potential therapeutic target for infection-related pregnancy complications.

Keywords: *T. gondii*, Infection, Decidual macrophage, Abnormal pregnancy, KLF6, LILRB4, Maternal-fetal tolerance,

Introduction

Toxoplasma gondii (*T. gondii*) is a globally distributed, obligate intracellular parasite that infects nearly one-third of the human population[1, 2]. Although infection is typically asymptomatic in immunocompetent individuals, *T. gondii* can pose serious risks to vulnerable populations, particularly pregnant women[3]. Infection during early gestation can lead to adverse pregnancy outcomes (APOs), including spontaneous abortion, stillbirth, and congenital toxoplasmosis[4, 5]. Given the profound implications for maternal–fetal health and population outcomes, there is an urgent need to elucidate the immune-molecular mechanisms underlying *T. gondii*-induced pregnancy complications. The immune microenvironment at the maternal-fetal interface is essential for the maintenance of pregnancy and is composed of diverse decidual immune cells, including decidual macrophages (dMφ), decidual natural killer (dNK) cells, and decidual dendritic cells (dDCs) [6, 7]. dMφ represent 20–30% of decidual leukocytes and are the second most abundant subset, playing critical roles in immune tolerance and gestational regulation [8, 9]. Dysfunctional dMφ has been associated with APOs, such as preeclampsia and spontaneous abortion [10, 11]. Our previous studies revealed that *T. gondii* infection disrupts dMφ homeostasis, contributing to these adverse outcomes [12, 13]. However, the molecular and cellular mechanisms by which infection disrupts dMφ function and leads to APOs remain incompletely understood.

Leukocyte immunoglobulin-like receptor B4 (LILRB4) is an inhibitory receptor predominantly expressed on macrophages and other myeloid cells [14]. Its cytoplasmic domain contains three immunoreceptor tyrosine-based inhibitory motifs (ITIMs), which, upon phosphorylation, recruit src homology domain type-2-containing tyrosine phosphatase (SHP)-1 or -2 to initiate an immunosuppressive signaling through targeted tyrosine dephosphorylation[15]. LILRB4 acts as a critical inhibitory receptor

and a central immune hub, governing myeloid cell-mediated homeostasis in health and tolerance/evasion in disease[16-18]. At the maternal-fetal interface, LILRB4 is highly expressed on dMφ, with peak levels during midgestation, essential for placental development and normal pregnancy[19]. Our previous study demonstrated that *T. gondii* infection significantly downregulated LILRB4 expression on dMφ, thereby impairing their function and leading to the compromise of maternal-fetal tolerance[20]. Nevertheless, the upstream regulatory mechanisms through which *T. gondii* mediates LILRB4 suppression remain poorly elucidated.

Normal dMφ manifest an immunotolerant phenotype, defined by elevated expression of immunosuppressive molecules like indoleamine 2,3-dioxygenase (IDO) alongside reduced levels of activation markers such as inducible nitric oxide synthase (iNOS) [21]. IDO, a heme-containing enzyme, is critical for maintaining immune tolerance and is essential for the maintenance of pregnancy[22, 23]. Our earlier work demonstrated that *T. gondii* infection impairs the function of dDCs and dMφ through downregulation of IDO[24, 25]. Conversely, sustained iNOS expression is often linked to inflammatory dysfunction and pregnancy complications [26]. We have previously demonstrated that *T. gondii* infection induces iNOS expression in dMφ. The concurrent downregulation of LILRB4 further exacerbates iNOS upregulation, thereby contributing to APOs[20]. However, these detailed mechanisms are still unknown. Given that the immunoinhibitory receptor LILRB4 is crucial for dMφ function and is downregulated upon *T. gondii* infection, we hypothesize that this downregulation compromises maternal-fetal tolerance by concomitantly suppressing the immunoregulatory molecule IDO and potentially dysregulating the activation marker iNOS, thereby shifting dMφ from a tolerant to a dysfunctional state.

In this study, we employed a combination of *in vitro* and *in vivo* models to investigate how LILRB4 mediates *T. gondii* infection-induced dMφ dysfunction, leading to APOs, and to explore the underlying molecular mechanism. Through bioinformatic prediction and screening, we identified the transcription factor KLF6 as a potential regulator of LILRB4. Using primary human dMφ and induced dM-like cells (MPA-pTHP-1), and an *in vivo* pregnant mouse model, we validated KLF6 as a direct transcriptional regulator of LILRB4 via EMSA and ChIP assays. Mechanistically, *T. gondii* infection suppresses LILRB4 expression through the pSTAT3(705)/KLF6 axis, as confirmed by inhibition and restoration experiments. Functionally, reduced LILRB4 expression, modeled by neutralizing antibody treatment *in vitro* and LILRB4 knockout *in vivo*, disrupted maternal-fetal tolerance through dysregulation of IDO and iNOS. Collectively, our findings establish a novel molecular framework linking *T. gondii*-mediated LILRB4 suppression to dMφ dysfunction and APOs, highlighting KLF6 as a critical mediator and potential therapeutic target for infection-associated pregnancy complications.

Results

KLF6 was located in the nucleus of normal dMφ and it was reduced after *T. gondii* infection

To identify transcription factors regulating LILRB4 expression, we first performed bioinformatics analyses using the UCSC and JASPAR databases (Figure 1A). Among the candidate factors, KLF6 emerged as a promising regulator based on its known roles in dMφ function and maternal-fetal tolerance. Using immunofluorescence (IF) and western blotting, we found that KLF6, which is predominantly localized in the

nucleus of normal primary human dMφ, was significantly downregulated upon *T. gondii* infection (Figure 1B – 1D). Consistently, flow cytometry analysis confirmed that KLF6 expression was significantly downregulated in both mouse (Figure 1E-1F) and human (Figure 1G-1H) dMφ after *T. gondii* infection (Supp. Figure 1).

T. gondii infection reduced LILRB4 expression on dMφ _via_ KLF6 suppression

To investigate the regulatory role of KLF6 on LILRB4 expression during *T. gondii* infection, we first detected the expression frequency of LILRB4 on dMφ after *T. gondii* infection. The results showed that the percentages of LILRB4 on human (Figure 2A and 2B) and mouse (Figure 2A and 2C) dMφ were significantly downregulated by flow cytometry. RT-qPCR showed that the mRNA level of LILRB4 was also significantly reduced by infection (Figure 2D). Next, we performed a correlation analysis between LILRB4 mRNA levels and KLF6 expression, indicating that they had a positive correlation (Figure 2E). Then, siRNAs targeting three distinct regions of the KLF6 mRNA (nucleotide positions 341, 831, and 926) were designed and subsequently transfected into the decidua-like macrophage cell line MPA-pTHP-1. Western blotting and IF showed that KLF6 knockdown significantly reduced LILRB4 expression in infected cells (Figure 2F and 2H, Supp. Figure 2). Further, the potential binding sites between the promoter region of LILRB4 and KLF6 were predicted by JASPAR sites (Table 1), and the preferential binding positions were -591 to -601 and -1967 to -1977 sites (Figure 2I). Electrophoretic mobility shift (EMSA) assay demonstrated that KLF6 preferentially bound the -591~-601 region of the LILRB4 promoter over the -1967~-1977 site, an interaction significantly diminished upon *T. gondii* infection (Figure 2J). Competitive EMSA and chromatin immunoprecipitation (ChIP)-qPCR analysis consistently confirmed that *T. gondii*

infection suppressed KLF6 binding to the -591–-601 region of the LILRB4 promoter (Figure 2K-2M).

T. gondii infection reduced LILRB4 expression on dMφ through the inhibition of STAT3 phosphorylation

A previous study reported that inhibition of STAT3 phosphorylation significantly downregulated LILRB4 expression[27]. To examine the role of STAT3 in LILRB4 suppression during *T. gondii* infection, we treated human and mouse dMφ with the STAT3 inhibitor stattic during infection (the experiment design *in vivo* is shown in Figure 3A). Flow cytometric analysis revealed that phosphorylation of STAT3 at tyrosine 705 (pSTAT3 (Y705)) in mouse (Figure 3B) and human dMφ (Figure 3C) was significantly inhibited. Meanwhile, static treatment significantly aggravated *T. gondii* infection-induced APOs, as evidenced by reduced fetal and placental weights and higher rates of fetal malformation (Figure 3D and 3E). More importantly, the expression levels of LILRB4 showed a significant downregulation in Stattic-treated and infected human (Figure 3F and 3G) or mouse (Figure 3F and 3H) dMφ compared to infected-only controls by flow cytometry. IF analysis indicated the mean fluorescence intensity (MFI) of LILRB4 on human dMφ was significantly reduced, and it was further weakened after Stattic treatment during infection (Figure 3I). Western blotting also showed that the protein expression of LILRB4 was significantly inhibited after STAT3 inhibition during infection (Figure 3J and 3K).

T. gondii infection downregulated LILRB4 expression on dMφ via the pSTAT3(Y705)-KLF6 pathway

To further investigate whether the downregulation of LILRB4 on dMφ by *T. gondii* infection was mediated by the suppression of the STAT3-KLF6 axis during infection,

the co-localization expression of KLF6 and pSTAT3 (705) was examined by IF. The results showed that KLF6 was localized in the nucleus, and pSTAT3 (Y705) showed dual localization, with significantly reduced expression levels of both proteins post-infection (Figure 4A). Further, co-immunoprecipitation assay revealed a direct interaction between pSTAT3 (Y705) and KLF6 in the nucleus of human dMφ (Figure 4B). Then, human and mouse dMφ were treated with a STAT3 inhibitor, Stattic; flow cytometric analysis showed significantly reduced KLF6 expression in inhibitor-treated and infected mouse (Figure 4C and 4D) or human (Figure 4E and 4F) dMφ compared to infected-only controls. Western blot showed that the nuclear protein of KLF6 in human dMφ was significantly downregulated after Stattic treatment during infection (Figure 4G and 4H). Next, dMφ were treated with the STAT3 inhibitor in combination with a KLF6 overexpression vector; the levels of LILRB4 in human dMφwere detected by western blotting. The results showed that KLF6 overexpression alone restored infection-mediated the downregulation of LILRB4 in dMφ, while STAT3 inhibition suppressed LILRB4 expression regardless of KLF6 status, indicating that STAT3 activity is essential for KLF6-mediated LILRB4 downregulation (Figure 4I and 4J).

LILRB4 downregulation during *T. gondii* infection suppresses IDO expression in dMφ

To examine the functional consequences of LILRB4 downregulation during infection, we reanalyzed single-cell RNA sequencing data from $CD14^+$ dMφ under normal and *T. gondii*-infected conditions[5]. LILRB4 was highly expressed in dMφ subsets 1, 2, and 5 (termed LILRB4-high dMφ) (Figure 5A and 5B). Then, differential expression genes (DEGs) analysis identified IDO as one of the top 20 DEGs (Figure 5C). GO analysis

further demonstrated that IDO was enriched in the top three immune-related pathways (Figure 5D). To validate these findings, we infected human and mouse dMφ with *T. gondii* in the presence or absence of a neutralizing LILRB4 antibody or genetic knockout. Flow cytometry revealed that *T. gondii* infection significantly reduced IDO expression in both human (Figure 5E and 5F) and mouse (Figure 5G and 5H) dMφ, with further reduction upon LILRB4 neutralization or deletion. Western blotting analysis further confirmed that both LILRB4 neutralization (Figure 5I-5J) and knockdown (Figure 5K-5L, Supp. Figure 3) led to decreased IDO protein expression in infected dMφ. Conversely, LILRB4 overexpression markedly restored infection-induced the reduction of IDO levels (Figure 5M and 5N).

LILRB4 downregulation reduces IDO expression via inhibition of SHP-1 phosphorylation in dMφ

To elucidate the signaling pathway through which LILRB4 modulates IDO expression during *T. gondii* infection, we assessed SHP-1/SHP-2 phosphorylation in dMφ treated with a neutralizing LILRB4 antibody. Western blotting analysis showed a significant reduction in pSHP-1(Y536), while total SHP-1, SHP-2, and pSHP-2 (Y548) levels remained unchanged (Figure 6A and 6B). Flow cytometry further confirmed decreased pSHP-1 (Y536) expression in infected dMφ, which was further diminished by LILRB4 blockade (Figure 6C and 6D). Immunoprecipitation assay demonstrated a direct interaction between LILRB4 and SHP-1 during infection (Figure 6E). Then, dMφ treated with the SHP-1 inhibitor TPI-1 led to a significant reduction in IDO expression (Figure 6F and 6G). Combined treatments revealed additive effects: SHP-1 inhibition and LILRB4 neutralization each suppressed IDO levels, and their combination further exacerbated this effect (Figure 6H and 6I). Notably, although

LILRB4 overexpression elevated IDO expression in infected dMφ, co-treatment with the SHP-1 inhibitor completely abrogated this rescue effect (Figure 6J and 6K).

T. gondii-induced LILRB4 downregulation suppresses IDO expression via the SHP-1/JAK/STAT1/IRF1 pathway in dMφ

IDO expression is regulated by multiple signaling pathways, including PI3K/AKT, noncanonical NF-κB (p52/RelB), and JAK/STAT[28-30]. To delineate the dominant pathway, infected human dMφ were treated with a STAT1 inhibitor (fludarabine), a PI3K inhibitor (LY294002), or a P52 inhibitor (SN52), respectively, followed by IDO analysis. The results showed that STAT1 inhibition significantly decreased IDO expression (Figure 7A and 7B), while P52 (Figure 7C and 7D) and PI3K inhibition (Figure 7E and 7F) had minimal effects. Flow cytometry confirmed IDO downregulation following STAT1 inhibition (Figure 7G and 7H). *T. gondii* infection suppressed pSTAT1 (Y701), and this suppression was further exacerbated by either SHP-1 inhibition or LILRB4 neutralization (Figure 7I and 7J). *In vivo* analysis recapitulated these observations: infected and LILRB4 knockout mice exhibited a more pronounced reduction in p-STAT1 (Y701) compared to infected wild-type controls (Figure 7K and 7L).

Moreover, IRF1 has been previously identified as essential for IDO induction[31]. To further define the signaling mechanism, infected dMφ were treated with fludarabine or the SHP-1 inhibitor TPI-1 in the context of LILRB4 overexpression. STAT1 inhibition reduced IRF1 and IDO expression, while LILRB4 overexpression increased them. Importantly, this LILRB4-induced upregulation was completely abolished by concurrent STAT1 inhibition (Figure 8A–8C). Further, IRF1 knockdown via siRNA in infected dMφ significantly reduced IDO expression (Supp. Figure 4). Combined

treatment with IRF1 knockdown and LILRB4 overexpression attenuated LILRB4-mediated IDO upregulation (Figure 8D and 8E). Similarly, SHP-1 inhibition reduced p-JAK2 (Y1007/1008), p-STAT1 (Y701), IRF1, and IDO expression levels. Although LILRB4 overexpression enhanced activation of these signaling molecules, SHP-1 inhibition completely reversed this effect (Figure 8F–8I).

***T. gondii*-induced LILRB4 downregulation promotes iNOS expression via the SHP-1/PI3K/c-Fos pathway in dMφ**

We previously demonstrated that *T. gondii* infection increases iNOS expression in dMφ by downregulating LILRB4[20]. Given the known involvement of PI3K and c-Fos in iNOS regulation[32, 33], we investigated this regulatory pathway; infected dMφ were treated with PI3K (NSC781406) or SHP-1 (TPI) inhibitors in combination with LILRB4 neutralization or overexpression. The results showed that SHP-1 inhibition and LILRB4 neutralization both significantly increased iNOS and PI3K expression (Figure 9A and 9B). Conversely, PI3K inhibition combined with LILRB4 overexpression markedly suppressed both iNOS and c-Fos levels (Figure 9C and 9D).

pSTAT3/KLF6-mediated LILRB4 suppression disrupts maternal-fetal tolerance by reciprocally modulating IDO and iNOS in dMφ during *T. gondii* infection

This study identifies a comprehensive molecular mechanism by which *T. gondii* infection disrupts dMφ-mediated maternal-fetal tolerance. Mechanistically, *T. gondii* infection suppresses STAT3 (Y705) phosphorylation, leading to reduced KLF6 expression and diminished binding to the LILRB4 promoter region (-591 to -601 bp). This results in downregulation of LILRB4 transcription and expression. Loss of LILRB4 in dMφ further impairs SHP-1 recruitment, which in turn inhibits IDO expression through suppression of the JAK2/STAT1/IRF1 signaling axis.

Concurrently, LILRB4 downregulation promotes iNOS expression via the SHP-1-PI3K-c-Fos pathway. Together, these findings establish a novel pSTAT3 – KLF6 – LILRB4 regulatory axis that links pathogen-induced transcriptional suppression to immune dysfunction at the maternal-fetal interface (Figure 10).

Discussion

LILRB4, a pivotal immune checkpoint receptor, serves as a master regulator of immunotolerance in various pathological contexts[34]. Nevertheless, its role in *T. gondii-induced* APOs remains relatively understudied. Although our earlier work showed that *T. gondii* infection disrupts maternal-fetal tolerance by downregulating LILRB4 in dMφ, dDCs, and decidual myeloid-derived suppressor cells (dMDSCs) [20, 35, 36], the upstream transcriptional regulation and downstream effector pathways were still unclear. Here, we identify for the first time that the transcription factor KLF6 is a key modulator of LILRB4 expression in dMφ during infection. We demonstrate that infection markedly suppresses KLF6 levels by inhibiting STAT3 phosphorylation at tyrosine 705. KLF6 binds directly to the LILRB4 promoter region (-591 to -601), and this interaction is significantly weakened upon infection, leading to reduced LILRB4 transcription and expression. Furthermore, loss of LILRB4 compromises dMφ function by downregulating the immunoregulatory molecule IDO and upregulating the pro-inflammatory enzyme iNOS, thereby disrupting maternal-fetal tolerance.

Previous studies have reported that cytokines such as interleukin-10 (IL-10) and type I interferons can upregulate LILRB4 expression in DCs or endothelial cells[37-39]. However, the transcriptional mechanisms underlying LILRB4 regulation have remained largely unexplored. KLF6, which is highly expressed in placental tissue,

plays an important role in reproductive health by regulating pregnancy-specific glycoproteins[40]. Recent studies have further shown that reduced KLF6 expression in trophoblasts impairs extravillous trophoblast differentiation and contributes to abnormal placental invasion[40, 41]. In macrophages, KLF6 has been shown to promote M2 polarization, reinforcing its role in immune regulation[42]. Consistent with these findings, we observed that KLF6 is highly expressed in the nuclei of dMφ and is significantly downregulated following *T. gondii* infection. siRNA-mediated knockdown of KLF6 markedly reduced LILRB4 expression, indicating a functional link between the two. Furthermore, EMSA and ChIP assays confirmed that KLF6 directly binds to the LILRB4 promoter region (positions -591 to -601), and this interaction was substantially weakened upon infection. Collectively, these results demonstrate that *T. gondii* infection downregulates LILRB4 expression and inhibits its transcriptional activity in dMφ, at least in part, by suppressing KLF6 expression.

Having established KLF6 as a direct transcriptional regulator of LILRB4, we next sought to identify the upstream signals controlling KLF6 itself during infection. Previous reports indicated a positive correlation between STAT3 activity and LILRB4 expression in dendritic cells[27], aligning with our earlier observation that *T. gondii* inhibits STAT3 phosphorylation and LILRB4 expression in decidual myeloid-derived suppressor cells[35]. This led us to hypothesize that STAT3 activation might be essential for maintaining LILRB4 expression in dMφ. Consistently, pharmacological inhibition of STAT3 phosphorylation significantly reduced LILRB4 levels both *in vitro* and *in vivo*, confirming the importance of STAT3 signaling. To further mechanistically connect STAT3 phosphorylation with KLF6 in the downregulation of LILRB4, we treated dMφ with a STAT3 inhibitor alone or in combination with KLF6 overexpression. We found that STAT3 inhibition significantly reduced both KLF6 and

LILRB4 expression in infected dMφ. While KLF6 overexpression alone rescued infection-mediated LILRB4 downregulation, this effect was completely abolished when STAT3 was simultaneously inhibited, demonstrating that STAT3 acts upstream of KLF6 and is indispensable for KLF6-mediated transcriptional activation of LILRB4. Furthermore, an immunoprecipitation assay confirmed a physical interaction between phosphorylated STAT3 and KLF6 during infection. This is consistent with reports that phosphorylation and activation of STAT3 in oligodendrocytes promotes KLF6 expression and cooperates with KLF6 to regulate target protein expression, without affecting KLF6 transcription[43]. Taken together, these data establish that *T. gondii* suppresses LILRB4 expression in dMφ primarily through an inhibition of the phosphorylation-dependent STAT3–KLF6 signaling axis.

IDO, a critical immunoregulatory enzyme and rate-limiting mediator of tryptophan metabolism[44, 45], is highly expressed in dMφ and essential for maintaining immune tolerance at the maternal-fetal interface[21]. To determine whether *T. gondii-induced* downregulation of LILRB4 influences IDO expression, we first analyzed single-cell RNA-sequencing data from our group, which revealed a strong positive correlation between LILRB4 and IDO transcript levels[5]. This correlation was functionally validated both *in vivo* and *in vitro*, where LILRB4 deficiency significantly suppressed IDO expression. Mechanistically, we found that LILRB4 downregulation during infection specifically inhibited the activation of SHP-1, but not SHP-2. Further immunoprecipitation assay and inhibitor treatment experiments confirmed that LILRB4 engages SHP-1 directly to regulate the expression of IDO, which is consistent with the finding that LILRB4 could recruit the SHP-1 or SHP-2 into the cell membrane46. Although IDO can be induced through multiple pathways—including PI3K/JNK, noncanonical NF-κB, and JAK/STAT[28-30], in our study,

pharmacological inhibitor screening identified the JAK/STAT1 axis as the predominant route through which LILRB4-SHP-1 signaling maintains IDO expression in infected dMφ. Thus, our results suggest that LILRB4 downregulation impairs IDO levels via suppression of the SHP-1/JAK/STAT1 pathway, revealing one key mechanism by which infection disrupts local immunotolerance.

IRF1, a transcription factor known to cooperate with STAT1 in driving IDO expression[31], emerged as a critical downstream effector in LILRB4-mediated immunoregulation. Building on our finding that LILRB4 sustains IDO via the JAK/STAT1 axis, we investigated whether IRF1 links this pathway to IDO transcription. The results showed that LILRB4 overexpression upregulated IDO, whereas IRF1 knockdown suppressed it, thereby establishing IRF1 as a necessary mediator of LILRB4 function. To further delineate the upstream signaling cascade, we systematically inhibited key nodes—SHP-1, JAK2, and STAT1—in combination with LILRB4 overexpression. The results demonstrated that LILRB4 downregulation during infection attenuates IDO expression sequentially through the SHP-1/JAK2/STAT1/IRF1 pathway. This work thus defines a linear modulatory circuit through which LILRB4 maintains IDO-dependent immunoregulation in dMφ, and its disruption during *T. gondii* infection directly contributes to the loss of maternal–fetal tolerance.

iNOS, a canonical marker of classically activated M1 macrophages, is a key driver of inflammatory responses and is closely associated with adverse pregnancy outcomes when its expression is sustained[26,47]. We have previously shown that *T. gondii* infection induces iNOS in dMφ and that the concomitant downregulation of LILRB4 further amplifies iNOS upregulation, contributing to the disruption of maternal–fetal tolerance[20]. However, the precise signaling mechanism linking LILRB4 loss to iNOS

induction remained undefined. In the present study, we delineate this pathway by demonstrating that LILRB4 downregulation during infection activates SHP-1, which in turn promotes phosphorylation of PI3K and subsequent upregulation of the transcription factor c-Fos, ultimately driving iNOS expression. This pathway reveals how LILRB4 deficiency coordinately yet divergently regulates immunoregulatory and pro-inflammatory programs in dMφ.

Conclusion

This study systematically elucidates, for the first time, the central mechanism by which *T. gondii* infection disrupts maternal-fetal immune tolerance, identifying LILRB4 downregulation in dMφ as a key driver of this process. We reveal that the infection specifically downregulates the expression of LILRB4, a pivotal immune checkpoint receptor on dMφ, by inhibiting STAT3 phosphorylation and its downstream transcription factor KLF6. This downregulation subsequently disrupts immune homeostasis at the maternal-fetal interface through the differential regulation of two SHP-1-dependent signaling axes: it suppresses the JAK2/STAT1/IRF1-mediated expression of IDO while concurrently activating the PI3K/c-Fos-driven production of iNOS. Our work not only delineates a complete molecular pathway underlying infection-related pregnancy complications but, more importantly, establishes LILRB4 as an actionable therapeutic hub linking pathogenic infection to APOs. This provides a novel perspective and a potential target for developing interventions aimed at restoring immune balance at the maternal-fetal interface.

Materials and Methods

Obtaining *T. gondii* tachyzoites

T. gondii tachyzoites were cultured in HEp-2 cells with Roswell Park Memorial Institute (RPMI)-1640 medium (PM150110, Pricella) plus 5% fetal bovine serum (FBS; F101, Vazyme) and 100 IU/ml penicillin and 100 IU/ml streptomycin (PB180120, Pricella). For the acquisition of *T. gondii* tachyzoites, the cells were removed by centrifugation at 300 × g for 5 min, and the supernatant was further centrifuged at 1500 × g for 7 min. Acquired *T. gondii* tachyzoites were left in the deposit and resuspended with appropriate MEM, and counted with a Neubauer chamber.

Animals

C57BL/6 mice (females: 6 – 8 weeks; males: 8 – 10 weeks) were obtained from Pengyue Laboratory Animal Technology Co., Ltd. (Jinan, China), while LILRB4-deficient (LILRB4$^{-/-}$) mice were acquired from Riken BioResource Center (Tsukuba, Japan). All mice were maintained under specific pathogen-free (SPF) conditions with controlled environmental parameters (22-26°C, 50 – 60% humidity, 12 h light/dark cycle). To establish the *T. gondii*-infected abnormal pregnancy model, female and male mice were co-housed overnight at a 2:1 ratio. Vaginal plug observation confirmed successful mating (gestational day 0, gd 0). Then, pregnant mice were randomly assigned to experimental groups: wild-type mice for normal control (NOR), *T. gondii*-infected group (INF), STAT3 inhibitor-treated group (Stattic or JSI-124, MCE), and STAT3 inhibitor+*T. gondii* group (Stattic+INF); LILRB4$^{-/-}$ mice for the LILRB4$^{-/-}$+T. *gondii* group (LILRB4$^{-/-}$+INF).

For *T. gondii* infection, at gd 8, the infected mice were intraperitoneally (*i.p.*) injected with 350 tachyzoites added into 200 μl phosphate buffer solution (PBS). The uninfected mice were injected with the same volume of PBS into the abdominal cavity.

For treatment with the STAT3 inhibitor, the mice were treated *i.p.* with 1 mg/kg JSI-124 in 200 μl sterile PBS at gd 8, 10, 12, respectively. At gd 14, the mice were euthanized.

Genotyping of LILRB4$^{-/-}$ Mice

Genomic DNA was extracted from the tail tissue of LILRB4$^{-/-}$mice using a tissue DNA extraction kit (GK0122, Generay). PCR amplification was initiated with a 3-minute denaturation at 95°C, followed by 35 cycles of denaturation (30 s at 95°C), annealing (30 s at 55°C), and extension (60 s at 72°C), concluding with a final extension step (5 min at 72°C). PCR products were resolved on 1.5% agarose gels, and fragment sizes were determined using Trans DNA marker I (100–700 bp; BM401-01, Transgene). DNA bands were visualized with GelStain (10,000×; GS101-01, Transgene). The primer sequences used for genotyping are as follows: LILRB4 P1, 5′-ACCGGTGGATGTGGAATGTGTG-3′; LILRB4 P2, 5′-GTCCTGGGTTCCAGAATAAGAC-3′; and LILRB4 P3, 5′-TCTGCTCTTAGGAAATTACAGAA-3′. Expected PCR product sizes were 260 bp for homozygous mutants, 371 and 260 bp for heterozygotes, and 371 bp for wild-type mice. Homozygous LILRB4$^{-/-}$ mice were continuously bred for all subsequent experiments.

Isolation of Decidual Cells from Mice

Mice from each experimental group were sacrificed at 6 days post-infection. Uteri and placentas were excised, minced into small fragments, and digested in 0.1% collagenase type IV (2091GR001, Biofoxx) containing 25 IU/ml DNase-I (D8071, Solarbio) at 37°C for 30 minutes. Single-cell suspensions were obtained by filtration through 48-μm sterile meshes. Mononuclear cells were isolated using Ficoll density gradient centrifugation with mouse lymphocyte separation medium (LTS1077-1, TBD

Science). Cells from the white interface layer were collected for flow cytometry.

Human Clinical Sample Collection

Decidual tissues were obtained from women at 8–10 weeks of gestation undergoing elective abortions without any clinical signs of genital tract infections. All samples were collected at the Department of Obstetrics and Gynecology, Yantai Mountain Hospital, and Yantai Affiliated Hospital of Shandong Medical and Pharmaceutical University. The collection protocols were approved by the Ethics Committee of Shandong Medical and Pharmaceutical University. Tissues were rinsed 5–8 times with sterile saline and maintained in RPMI-1640 medium supplemented with 100 IU/ml penicillin and 100 IU/ml streptomycin.

Isolation of Human dMφ

Decidual tissues were minced and digested enzymatically in RPMI-1640 containing 0.1% collagenase type IV and 25 IU/ml DNase-I at 37°C for 40 min. Single-cell suspensions were filtered through a 48-μm mesh and centrifuged using Lymphocyte Separation Medium at 770 × g for 20 minutes at 20°C. Mononuclear cells were collected from the interface, erythrocytes were lysed (R1010, Solarbio), and stromal cells were depleted. $CD14^+$ dMφ were isolated using a human CD14 positive selection kit (18058, Stem Cell Science) following the manufacturer's protocol. Cell purity exceeded 95% in all experiments.

Experimental Design and Treatments

Isolated dMφ were allocated into five experimental groups: uninfected control (NOR), *T. gondii*-infected (INF), Stattic-treated (STAT3 inhibitor, HY-13818, MCE), Stattic+INF, and LILRB4-neutralized +INF (Neu+INF). For inhibitor or neutralizing treatments, dMφ were pre-treated with 10 μg/ml Stattic or 10 μg/ml anti-LILRB4 antibody (16-5139-85, eBioscience) for 2 hours before infection. *T. gondii* infection

was performed at a parasite-to-cell ratio of 3:1. All cultures were maintained in RPMI-1640 supplemented with 10% FBS and 100 IU/ml penicillin and streptomycin for 24 hours at 37°C before downstream analysis.

Induction of a dMφ-like Cell Line (MPA-pTHP-1)

The human THP-1 monocytic cell line (Procell Life Science) was maintained in RPMI-1640 medium supplemented with 10% FBS and 1% antibiotic-antimycotic solution. To generate dMφ-like cells, THP-1 cells (5-8×10^6 cells/10-cm dish) were differentiated using 50 nM phorbol 12-myristate acetate (PMA; HY-18739, MCE) for 6 hours, followed by 72 hours of culture in medium containing 0.1 μM medroxyprogesterone acetate (MPA, HY-B0469, MCE) [48]. After a 24-hour resting period in fresh medium, the resulting MPA-pTHP-1 cells were used for mechanistic studies involving inhibitor treatments, siRNA knockdown, or plasmid overexpression by western blotting analysis.

Flow Cytometry

In vivo staining

Mouse mononuclear cells were stained with fluorochrome-conjugated mAbs (see Supplementary Information 1). For surface LILRB4 detection, cells were incubated with anti-F4/80 and anti-LILRB4 antibodies at 4°C for 40 min in the dark, washed twice with PBS, and resuspended in 500 μl PBS. For intracellular targets including IDO, pSTAT3(Y705), pSHP-1(Y536), and pSTAT1(Y701), as well as nuclear (KLF6), F4/80-stained cells were fixed and permeabilized using Fix/Perm buffer (88-8824 or 00-5523, Thermo Fisher) for 60 minutes, followed by staining with the appropriate intracellular antibodies (4°C, 60 minutes, dark).

In vitro assays

Human decidual mononuclear cells were stained with anti-CD14 and anti-LILRB4

antibodies under the same conditions described above. Intracellular staining was conducted using the same protocol. All samples were analyzed using a BD FACSCanto II flow cytometer (Becton Dickinson).

Real-time Quantitative PCR (qPCR)

Total RNA was extracted from dMφ using Triquick reagent (R1100, Solarbio) and reverse-transcribed into cDNA using the Transcriptor First Strand cDNA Synthesis Kit (R0202, LABELLAB). qPCR amplification was performed using ChamQ Blue Universal SYBR qPCR Master Mix (Q312-02, Enzyme) on a Roche LightCycler® 96 system. Gene expression levels were normalized to GAPDH. Primer sequences for KLF6, STAT3, and LILRB4 are provided in Supplementary Information 1. Relative expression levels were analyzed using LightCycler® 96 SW1.1 software.

Isolation of Nuclear and Cytoplasmic Proteins

At least 2 × 10^7 dMφ from the NOR, INF, Stattic, and Stattic+INF groups were harvested and washed twice with cold PBS. Cytoplasmic and nuclear protein fractions were isolated using the Cell Fractionation kit (EX1470, Solarbio) following the manufacturer's protocol. After centrifugation at 700 × g for 10 min at 4℃, supernatants were discarded, and cell pellets were resuspended in 200 µl cytoplasmic protein extraction reagent. Suspensions were vortexed for 5 seconds and incubated on ice for 10 – 15 min. Next, 50 µl of extraction reagent B was added, followed by vortexing for 5 seconds and incubation on ice for 1 minute. Lysates were centrifuged at 14,000 × g for 10 min at 4 °C to collect cytoplasmic proteins. Insoluble nuclear pellets were resuspended in 50 µl nuclear extraction reagent, vortexed every 5 minutes for 20 seconds (total 30 min on ice), and then centrifuged at 14,000 × g for 10 min at 4 °C. Supernatants containing nuclear proteins were mixed with 1× loading buffer and boiled for 10 minutes at 100°C for western blotting analysis.

Western blotting.

dMφ (1×10^7 cells/group) were lysed in RIPA buffer (Solarbio, R0020) containing 1× phenylmethylsulfonyl fluoride (PMSF; P0100, Solarbio) and protein phosphatase inhibitor (B15001, Selleck) on ice (45–60 min), followed by centrifugation (12,000×g, 20 min, 4°C). Protein concentrations were determined by the bicinchoninic acid assay (PC0020, Solarbio). Samples were denatured (5×loading buffer, 8 min, 100°C), separated by SDS-PAGE, and transferred to polyvinylidene fluoride (PVDF, ISEQ00010, Merck Millipore). After blocking (5% nonfat milk, 2 h), membranes were incubated with primary antibodies (Supplementary Information 1, 4°C overnight) followed by HRP-conjugated secondary antibodies (2 h, RT). Protein bands were detected using an ECL reagent (BL520B, Biosharp) and imaged using the Bio-Rad ChemiDoc XRS^+ System. Band intensities were quantified (ImageJ) relative to GAPDH. All experiments were repeated ≥3 times independently.

Immunoprecipitation (IP) assay

To examine the interactions of LILRB4 with SHP-1 or pSTAT3(705) with KLF6, an IP assay was performed. Briefly, 1×10^7 purified human dMφs from the NOR, INF, and Neu+INF groups were collected and lysed with cell lysis buffer (R0020, Solarbio). The cell lysates were preabsorbed with protein A/G agarose beads for 1 h at 4°C with rotation. The protein concentration was measured via a bicinchoninic acid assay (PC0020, Solarbio). According to the instructions of the IP kit (EA-IP-K007M, Elabscience), twenty percent of the whole-cell lysate was isolated and regarded as the input group, with 5× loading buffer boiling for 10 min at 100°C. The remaining extracts were incubated with anti-pSTAT3(705) or anti-SHP-1 antibodies overnight with rotation at 4°C, followed by incubation with protein A/G agarose beads overnight at 4°C. The beads were washed with lysis washing buffer 3 times and

denatured at 100°C for 10 min. The denatured protein samples were subjected to KLF6 and LILRB4 detection via western blot analysis.

Electrophoretic mobility shift assay (EMSA)

To investigate the KLF6-mediated transcriptional regulation of LILRB4 in dMφ during *T. gondii* infection, biotin-labeled oligonucleotides spanning KLF6 binding sites (591–601 or 1927–1937 bp upstream of the LILRB4 promoter) were synthesized and incubated with nuclear extracts from dMφ (NOR and INF groups), which were prepared using a nuclear extraction kit (EX1470, Solarbio). Following the EMSA protocol (GS009, Beyotime), protein–DNA complexes were resolved on 5% native polyacrylamide gels, transferred to nylon membranes, and UV-crosslinked (540 nm). The membranes were blocked for 2 h at room temperature, probed with an anti-KLF6 antibody (A23220, Proteintech) for another 2 h, washed, and incubated with a secondary antibody for 40 min at room temperature. Finally, signals were detected via a ChemiDoc XRS+ system (Bio-Rad). The oligonucleotide sequences used were as follows: KLF6-1 (5'-AGTTGAGGGGACTTTCCCAGGC-3') and KLF6-2 (5'-AGCTCGCGTGACTCAGCTG-3').

Chromatin immunoprecipitation (ChIP)-qPCR

ChIP assays were performed via a Pierce Magnetic ChIP Kit (26157, Thermo Fisher Scientific) following the manufacturer's protocol. Briefly, dMφ from the normal and infected groups were crosslinked with 1.5% paraformaldehyde at room temperature for 20 min, quenched with 125 mM glycine for 5 min, and then washed with ice-cold PBS containing 1× protease inhibitor. Chromatin was digested with micrococcal nuclease (150–900 bp fragments) and sonicated (20 cycles: 5 sec ON/20 sec OFF). For immunoprecipitation, the chromatin was incubated overnight at 4°C with an anti-

KLF6 monoclonal antibody, followed by incubation with protein G agarose beads for 2 h. The beads were subsequently washed with low- and high-salt buffers. After elution (65°C, 30 min), crosslinking was reversed via the addition of 5 M NaCl/proteinase K (65°C, 2 h). DNA was purified via spin columns, with 10% input used as a control. qPCR was performed via the use of ChamQ SYBR Master Mix (Q312-02, Enzyme) on a Lightcycler96 system. The primers used to target the LILRB4 promoter region (-591 to -601 bp; designed via Primer3) are listed in the supplementary information 1. The data were normalized to the input data and compared to the IgG control data.

Immunofluorescence imaging

Purified human dM φ from all experimental groups were fixed in 4% paraformaldehyde (15 min), blocked with goat serum (1 h), and incubated overnight at 4°C with primary antibodies: anti-LILRB4 (sc-515288, Santa Cruz), anti-pSTAT3(705) (AP0705, ABclonal), and anti-KLF6 (67297-1-Ig, Proteintech). Corresponding secondary antibodies were used: DyLight 649-goat anti-rabbit IgG (A23620, Abbkine) for LILRB4, DyLight 488-goat anti-rabbit IgG (A23220, Abbkine) for pSTAT3, and DyLight 649-goat anti-mouse IgG (A23610, Abbkine) for KLF6 (37°C, 1 h). Nuclei were counterstained with DAPI (15 min), and images were acquired using a Leica confocal microscope.

Prediction of potential oligonucleotide sequences between KLF6 and the LILRB4 promoter

Bioinformatic analysis via the UCSC (http://genome.ucsc.edu/) and JASPAR (https://jaspar.elixir.no/) platforms identified several candidate transcription factors for human LILRB4.

Statistical analyses

Statistical analyses were performed via GraphPad Prism 9 (GraphPad Software, San Diego, CA, USA). The data are expressed as the means ± Standard Deviation (SD). Comparisons between two groups were assessed via two-tailed unpaired Student's t test, whereas multiple-group comparisons were analyzed via one-way analysis of variance (ANOVA) followed by appropriate post hoc tests. A p value < 0.05 was considered statistically significant, with the following thresholds: $*p < 0.05$, $p < 0.01$, and $*p < 0.001$.

Author Contributions

Z.D.L, X.M.H designed the experiments; R.T.M, T.Y.J, and Z.D.Z contributed to sample collection; Z.D.L, F.Z, and X.B.L did the experiment; Z.D.L, T.Y.J, F.Z, Z.D.Z, X.B.L, L.Q.R, Y.Z.J, H.X.Z, and X.M.H analyzed the data; Z.D.L wrote the manuscript. X.M.H revised the manuscript and is the corresponding author. All authors read and approved the final manuscript.

Acknowledgments

This work was supported by funds from the Natural Science Foundation of Shandong province (NO. ZR2021QH039, ZR2021MH310), the National Natural Science Foundation of China (NO. 81871680, NO. 81672049). We would like to thank TopEdit (www.topeditsci.com) for its linguistic assistance during the preparation of this manuscript. The graphical abstract was supported by BioRender.com

Ethical Statement

The human sample collection procedures for this study were approved by the Shandong Medical and Pharmaceutical University Ethics Committee (approval number 2021--014). Pregnant women who were diagnosed with early normal

gestation and who underwent voluntary abortions were enrolled in this study. All participants provided written informed consent for the collection of samples and subsequent analysis and that they did not have any complications of infectious disease. They also had no previous infection with *T. gondii*. The animal experiments in this study were carried out in strict accordance with the recommendations in the Guide for the Care and Use of Laboratory Animals of Shandong Medical and Pharmaceutical University (permit number F-KY-0022-20220325-01). All procedures were performed under sodium pentobarbital anesthesia, and all efforts were made to minimize the suffering of the animals.

Conflicts of Interest

The authors declare no competing interests.

Data Availability Statement

All data are available within the main text and Supporting Information. The RNA-seq raw data described in the present study have been submitted to the GEO database. Accession number is GSE254302.

References

1. Aguirre, A. A., Longcore, T., Barbieri, M., et al. The One Health Approach to Toxoplasmosis: Epidemiology, Control, and Prevention Strategies. *EcoHealth.* **16**, 378-390 (2019).
2. Megli, C. J., & Coyne, C. B. Infections at the maternal-fetal interface: an overview of pathogenesis and defence. Nature reviews. *Microbiology*. **20,** 67-82 (2022).
3. Teimouri, A., Goudarzi, F., Goudarzi, K., et al. *Toxoplasma gondii* Infection in Immunocompromised Patients: A Systematic Review and Meta-Analysis. *Frontiers in microbiology*. **8,** 389 (2022).
4. Conceição, A. R., Belucik, D. N., Missio, L., et al. Ocular Findings in Infants with Congenital Toxoplasmosis after a Toxoplasmosis Outbreak. *Ophthalmology.* **128,** 1346-1355 (2021).
5. Fu, T., Wang, X., Zhao, X., et al. Single-cell transcriptomic analysis of decidual immune cell landscape in the occurrence of adverse pregnancy outcomes induced by *Toxoplasma gondii* infection. *Parasites & vectors.***17,** 213 (2024).
6. Bian, Q., & Fu, B.. Immunological microenvironment at the maternal-fetal interface. *Journal of reproductive immunology.* **151,** 103632 (2022).
7. Greenbaum, S., Averbukh, I., Soon, E., et al. "A spatially resolved timeline of the human maternal-fetal interface." *Nature*. **619,** 595-605 (2023).
8. Liu, H., & Zhang, L. Decidual macrophage subsets and polarization puzzle during the human early pregnancy. *Frontiers in immunology*. **16,** 1610891 (2025).
9. Yang, D., Thiele, K., Yin, T., & Diao, L. Macrophage clock of pregnancy: circadian and metabolic control of decidual macrophage. *Seminars in immunopathology*. **47,** 30 (2025).
10. Rong, M., Yan, X., Zhang, H., et al. Dysfunction of Decidual Macrophages Is a Potential Risk Factor in the Occurrence of Preeclampsia. *Frontiers in immunology*. **12,** 655655 (2021).
11. Zhao, Q. Y., Li, Q. H., Fu, Y. Y., et al. Decidual macrophages in recurrent spontaneous abortion. *Frontiers in immunology*. 13, 994888 (2022).
12. Wang, Q., Cao, Y., Ye, S., et al. Trem2/Syk/PI3K axis contributes to the host protection against *Toxoplasma gondii*-induced adverse pregnancy outcomes via modulating decidual macrophages. *PLoS pathogens*. **20,** e1012543 (2024).
13. Cui, L., Wang, Y., Ren, L., et al. Effect of B7-H4 downregulation induced by *Toxoplasma gondii* infection on dysfunction of decidual macrophages contributes to adverse pregnancy outcomes. *Parasites & vectors*. **15,** 464 (2022).
14. Xiang, Z., Yin, X., Wei, L., et al. LILRB4 Checkpoint for Immunotherapy: Structure, Mechanism and Disease Targets. *Biomolecules*. **14,** 187 (2024).
15. Deng, M., Gui, X., Kim, J., et al. LILRB4 signalling in leukaemia cells mediates T cell suppression and tumour infiltration. *Nature*. **562,** 605-609 (2018) .
16. Gong, L., Sun, H., Liu, L., et al. LILRB4 represents a promising target for immunotherapy by dual targeting tumor cells and myeloid-derived suppressive cells in multiple myeloma. *Haematologica*. **109,** 3650-3669 (2024) .
17. Yang, T., Qian, Y., Liang, X., et al. LILRB4, an immune checkpoint on myeloid cells." *Blood science* (Baltimore, Md.). **4,** 49-56 (2022).
18. Sharma, N., Atolagbe, O. T., Ge, Z., et al. LILRB4 suppresses immunity in solid tumors and is a potential target for immunotherapy. *The Journal of experimental medicine*. 218, e20201811 (2021).
19. Matsumoto, Y., Wang, L. L., Yokoyama, W. M., et al. Uterine macrophages express the gp49B inhibitory receptor in midgestation. *Journal of immunology*. **166,** 781-6 (2001).
20. Li, Z., Zhao, M., Li, T., et al. Decidual Macrophage Functional Polarization during Abnormal Pregnancy due to *Toxoplasma gondii*: Role for LILRB4. *Frontiers in immunology*. **8,** 1013 (2017).
21. Huang, H. L., Yang, H. L., Lai, Z. Z., et al. Decidual IDO^{+} macrophage promotes the proliferation and restricts the apoptosis of trophoblasts. *Journal of reproductive*

immunology. **148,** 103364 (2021).
22. Chang RQ, Li DJ, Li MQ. The role of indoleamine-2,3-dioxygenase in normal and pathological pregnancies. *American journal of reproductive immunology*. **79,** e12786. (2018).
23. Munn DH, Mellor AL. Indoleamine 2,3 dioxygenase and metabolic control of immune responses. *Trends in immunology*. **34,** 137-43 (2013).
24. Sun, X., Xie, H., Zhang, H., et al. B7-H4 reduction induced by *Toxoplasma gondii* infection results in dysfunction of decidual dendritic cells by regulating the JAK2/STAT3 pathway. *Parasites & vectors*. **15,** 157 (2022).
25. Xie, H., Li, Z., Zheng, G., et al. Tim-3 downregulation by *Toxoplasma gondii* infection contributes to decidual dendritic cell dysfunction. *Parasites & vectors*. **15,** 393 (2022).
26. Al-Azemi, M., Refaat, B., Amer, S., et al. The expression of inducible nitric oxide synthase in the human fallopian tube during the menstrual cycle and in ectopic pregnancy. *Fertility and sterility*. **94,** 833-40 (2010).
27. Dáňová, K., Klapetková, A., Kayserová, J., et al. NF-κB, p38 MAPK, ERK1/2, mTOR, STAT3 and increased glycolysis regulate stability of paricalcitol/dexamethasone-generated tolerogenic dendritic cells in the inflammatory environment. *Oncotarget*. **6,** 14123-38 (2015).
28. Wang, D., Saga, Y., Sato, N., et al. The hepatocyte growth factor antagonist NK4 inhibits indoleamine-2,3-dioxygenase expression via the c-Met-phosphatidylinositol 3-kinase-AKT signaling pathway. *International journal of oncology*. **48,** 2303-9 (2016).
29. Wang, Y., Zhao, X., Li, Z., et al. Decidual natural killer cells dysfunction is caused by IDO downregulation in dMDSCs with *Toxoplasma gondii* infection. *Communications biology*. **7,** 669 (2024).
30. Snyder, M., Wang, Z., Lara, B., et al. "The aryl hydrocarbon receptor controls IFN-γ-induced immune checkpoints PD-L1 and IDO via the JAK/STAT pathway in lung adenocarcinoma." *Journal of immunology (Baltimore, Md. : 1950)* vol. 214,3 (2025): 413-432. doi:10.1093/jimmun/vkae023
31. Ebina, T., Ri, M., Marumo, Y., et al. Targeting Overexpressed IDO in Stromal Cells as a Potential Therapeutic Strategy in Multiple Myeloma. *Cancer science*. **117,** 325-334 (2026).
32. Singh, S. B., Braun, C. A., Carroll-Portillo, A., et al. Sulfate-Reducing Bacteria Induce Pro-Inflammatory TNF-α and iNOS via PI3K/Akt Pathway in a TLR 2-Dependent Manner. *Microorganisms*. **12,** 1833 (2024).
33. Jang, S. Y., Kim, S. Y., Song, H. A., et al. Protective effect of hydrangenol on lipopolysaccharide-induced endotoxemia by suppressing intestinal inflammation. *International immunopharmacology*. **125(Pt A),** 111083 (2023).
34. Wang, X., Li, L., Liu, D., et al. LILRB4 as a novel immunotherapeutic target for multiple diseases. *Biochemical pharmacology*. **233,** 116762 (2025).
35. Li, Y., Guo, J., Zhang, H., et al. LILRB4 regulates the function of decidual MDSCs via the SHP-2/STAT6 pathway during Toxoplasma gondii infection. *Parasites & vectors*. **16,** 237 (2023).
36. Zhan, S., Zheng, J., Zhang, H., et al. LILRB4 Decrease on uDCs Exacerbate Abnormal Pregnancy Outcomes Following *Toxoplasma gondii* Infection. *Frontiers in microbiology*. **9,** 588 (2018).
37. Vlad, G., Chang, C. C., Colovai, A. I., et al. Membrane and soluble ILT3 are critical to the generation of T suppressor cells and induction of immunological tolerance. *International reviews of immunology*. **29,** 119-32 (2010).
38. Buckland M, Lombardi G. Aspirin and the induction of tolerance by dendritic cells. *Handbook of experimental pharmacology*. **188,** 197-213 (2009).
39. Penna, G., Roncari, A., Amuchastegui, S., et al. Expression of the inhibitory receptor ILT3 on dendritic cells is dispensable for induction of $CD4^{+}Foxp3^{+}$ regulatory T cells by 1,25-dihydroxyvitamin D3. *Blood*. **106,** 3490-7 (2005).
40. Blanchon, L., Bocco, J. L., Gallot, D., et al. Co-localization of KLF6 and KLF4 with pregnancy-specific glycoproteins during human placenta development. *Mechanisms of*

development vol. **105,** 185-9 (2001).
41. Miranda, A. L., Kourdova, L. T., Racca, A. C., et al. Krüppel-like factor 6 participates in extravillous trophoblast cell differentiation and its expression is reduced in abnormally invasive placenta. *FEBS letters*. **596,**1700-1719 (2022).
42. Bi, J., Zeng, X., Zhao, L., et al. miR-181a Induces Macrophage Polarized to M2 Phenotype and Promotes M2 Macrophage-mediated Tumor Cell Metastasis by Targeting KLF6 and C/EBPα. *Molecular therapy*. *Nucleic acids.* **5,** e368. (2016).
43. Laitman, B. M., Asp, L., Mariani, J. N., et al.The Transcriptional Activator Krüppel-like Factor-6 Is Required for CNS Myelination. *PLoS biology*. **14,** e1002467 (2016).
44. Guo, Y., Liu, Y., Wu, W., et al. Indoleamine 2,3-dioxygenase (Ido) inhibitors and their nanomedicines for cancer immunotherapy. *Biomaterials*. **276,** 121018 (2021).
45. Moon, Y. W., Hajjar, J., Hwu, P., et al. Targeting the indoleamine 2,3-dioxygenase pathway in cancer. *Journal for immunotherapy of cancer*. **3,** 51 (2015).
46. Liu, H., Yang, J., Zhang, J., et al. Molecular regulatory mechanism of LILRB4 in the immune response. *Central-European journal of immunology*. **48,** 43-47 (2023).
47. Kieler M, Hofmann M, Schabbauer G. More than just protein building blocks: how amino acids and related metabolic pathways fuel macrophage polarization. *The FEBS journal*. **288,** 3694-3714 (2021).
48. Tsai, Y. C., Tseng, J. T., Wang, C. Y., et al. Medroxyprogesterone acetate drives M2 macrophage differentiation toward a phenotype of decidual macrophage. *Molecular and cellular endocrinology*. **45,** 274-83 (2017).

Figure legends

Figure 1 *T. gondii* infection suppressed the expression of the transcription factor KLF6 in dMφ

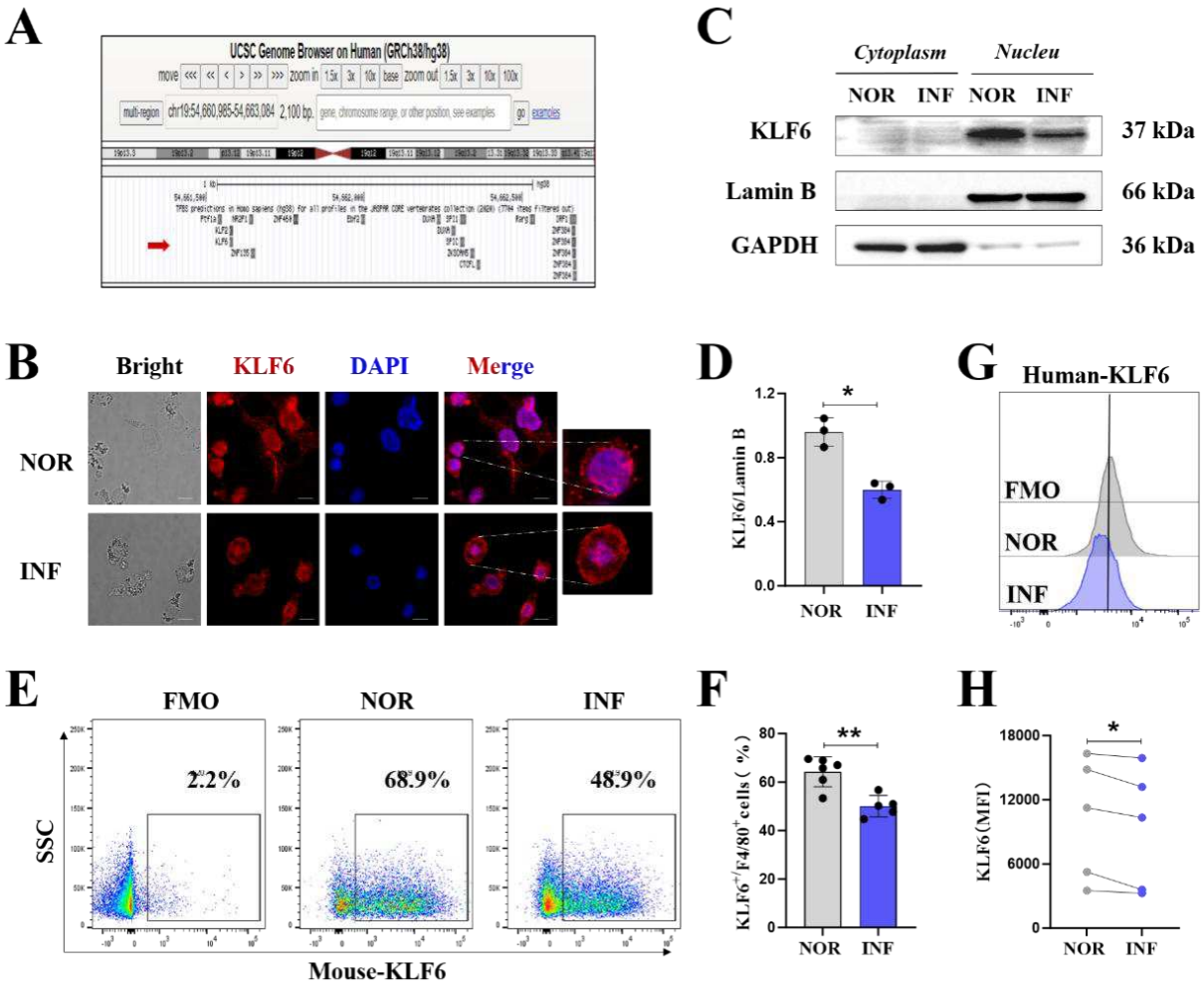

(A) Transcription factors predicted to target the LILRB4 gene via UCSC (http://genome.ucsc.edu/). **(B)** Representative confocal images of KLF6 in human dMφs from the NOR and INF groups (n ⩾ 3). The data represent the mean ± SD. P values were obtained via paired one-tailed Student's t tests. NOR, normal human dMφ; INF, *T. gondii*-infected human dMφ. **(C&D)** Western blot analysis and quantification of KLF6, GAPDH, and Lamin B in the cytoplasm and nucleus extracts of human dMφs in the NOR and INF groups via ImageJ (n ⩾ 3). GAPDH and lamin B were used as internal controls for the cytoplasm and nucleus, respectively. The data are presented as the means ± SDs. P values were obtained via paired two-tailed Student's t tests. Representative flow cytometry data for the MFI of mouse **(E&F)** or human **(G&H)** KLF6 in dMφs in the NOR and INF groups.

Figure 2 *T. gondii* infection inhibit KLF6 expression in dMφ

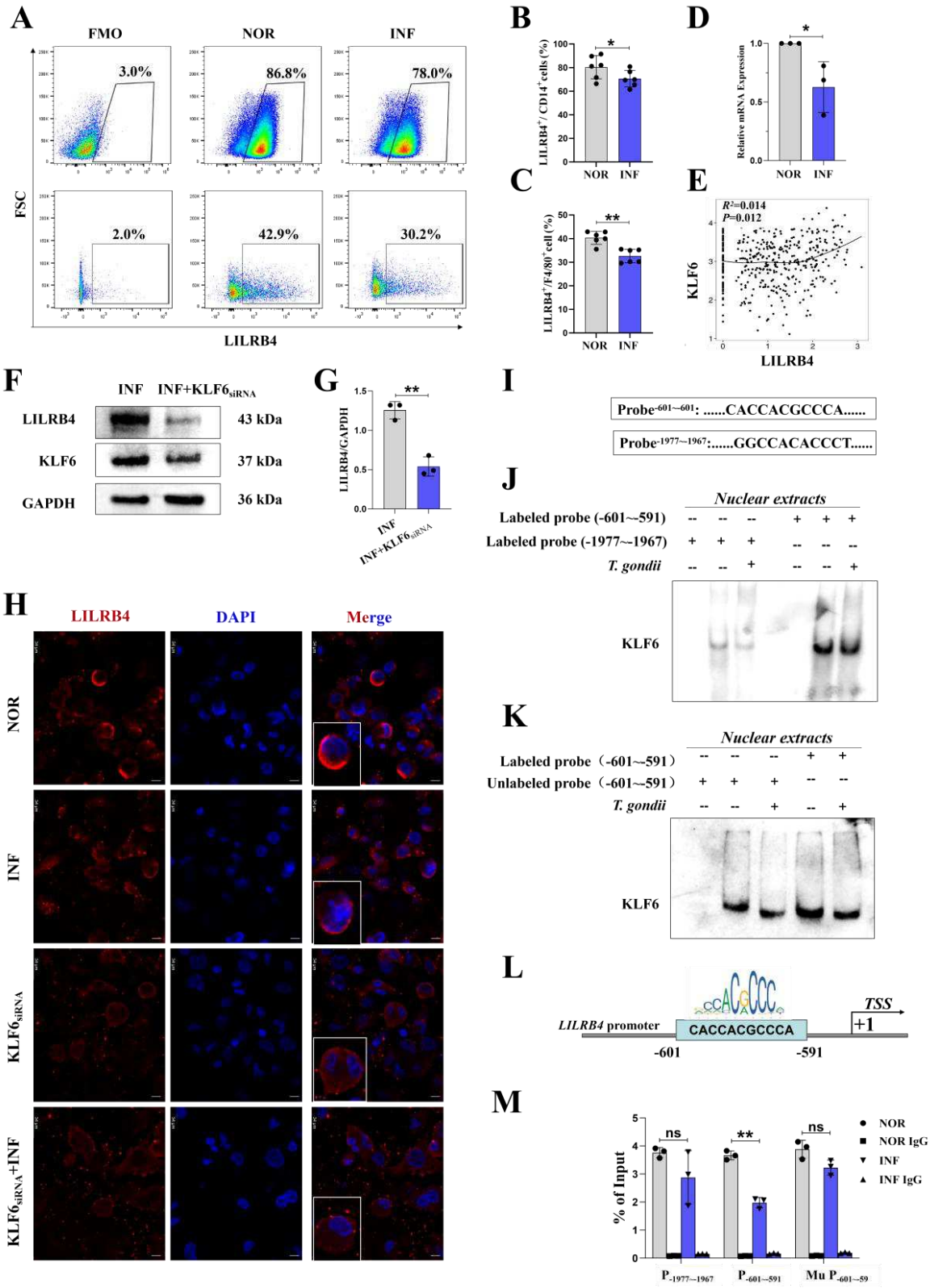

Representative data and the results of the statistical analysis of flow cytometry data for the frequency of LILRB4 on human **(A&B)** or mouse **(A&C)** dMφs in the NOR

and INF groups (n = 4–9). The data are presented as the means ± SDs. The P value was obtained via one-way analysis of variance (ANOVA) with NOR versus INF. **(D)** The mRNA levels of LILRB4 in the NOR and INF groups were detected by q-PCR analysis. **(E)** Correlation analysis was performed between LILRB4 and KLF6 expression in dMφs. **(F&G)** Western blot analysis of LILRB4 of human dMφ treated with three different KLF6siRNAs (INF, $KLF6_{siRNA341}$+INF, $KLF6_{siRNA831}$+INF, $KLF6_{siRNA926}$+INF) during *T. gondii* infection. GAPDH was regarded as an internal reference. **(H)** Representative confocal images of LILRB4 expression in human dMφs in the NOR, INF, $KLF6_{siRNA926}$ and $KLF6_{siRNA926}$+INF groups (n = 3). **(I)** Predicted KLF6 binding sites and binding scores on the LILRB4 promoter. **(G)** EMSA showing KLF6 binding to biotin-labeled oligonucleotide sequences corresponding to positions -591 to -601 and -1967 to -1977 on the LILRB4 promoter, using nucleus extracts from NOR and INF dMφ. Neg, negative control. **(K)** Competitive EMSA assay of KLF6 binding to the biotin-labeled -591–-601 oligonucleotide sequence in NOR and INF dMφ nuclear extracts. "Neg" indicates no binding to the probe; NORc and INFc represent competition assays using unlabeled probes before biotin-labeled probe incubation. NOR and INF indicate direct binding to the labeled probe. **(L)** Schematic of the KLF6 binding site (-591–-601) on the LILRB4 promoter, the binding sequence is CACCACGCCCA. **(M)** ChIP-qPCR analysis of KLF6 binding to the -591–-601 region of the LILRB4 promoter. ChIP was performed using an anti-KLF6 antibody, followed by qPCR with three primers targeting this region. Data are representative of at least three independent experiments. Results are expressed as the mean ± SD. **P*-values were calculated using a paired two-tailed Student's t-test. NOR, normal human dMφ; INF, *T. gondii*-infected dMφ; NOR IgG and INF IgG, isotype controls for respective groups.

Figure 3 *T. gondii* infection downregulates LILRB4 expression in dMφ via the inhibition of the phosphorylation of STAT3

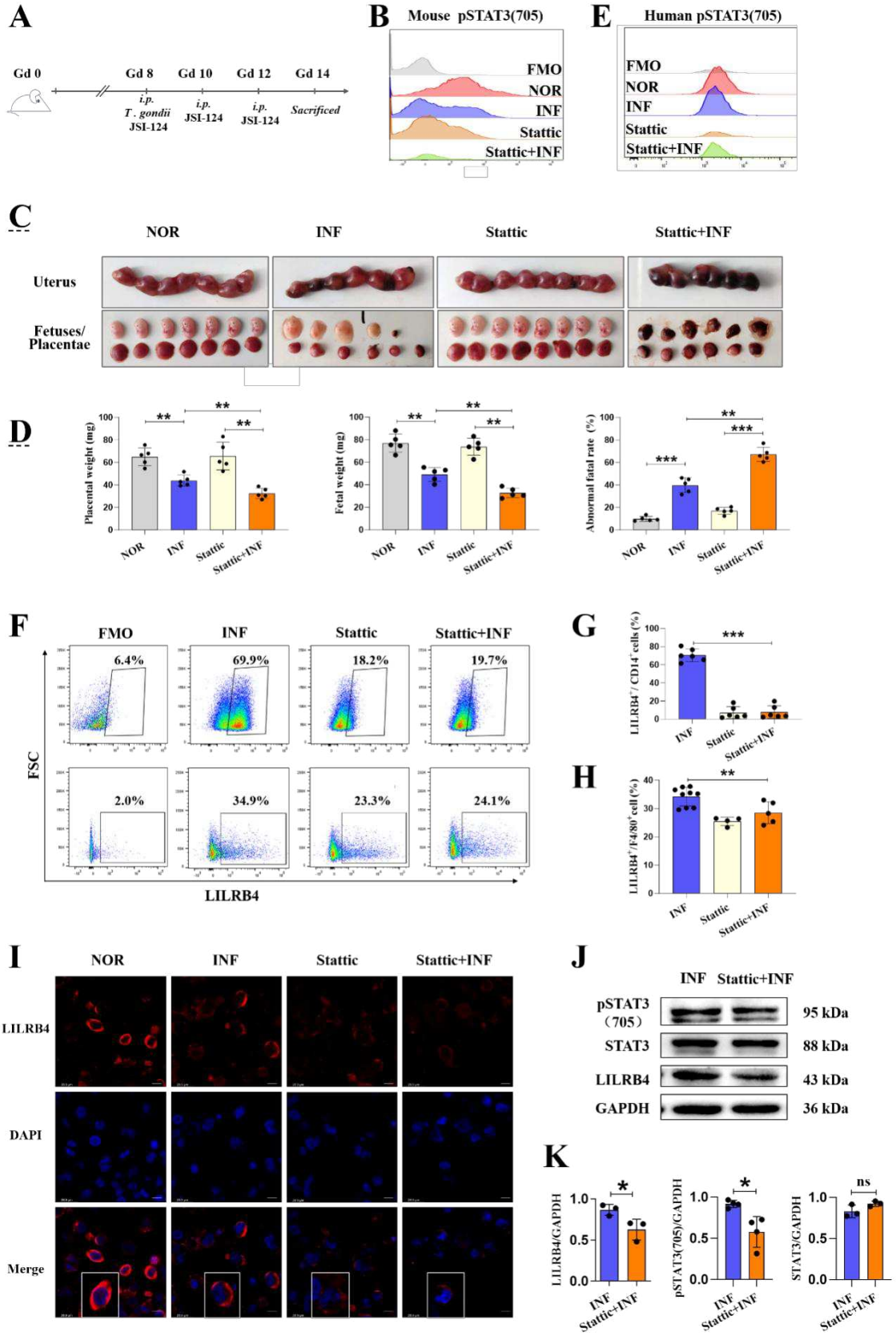

(A) Experimental design of after treatment with the STAT3 inhibitor JSI-124 in a *T. gondii*-infected murine model. **(B)** Representative flow cytometry data for the MFI of mouse pSTAT3(705) in dMφs treated with a STAT3 inhibitor (NOR, INF, Stattic, and Stattic+INF groups). **(C & D)** Uterine morphology and fetal-placental development in uninfected, infected, STAT3 inhibitor-treated, and STAT3 inhibitor plus infected mice. Placental and fetal weights and abnormal fetal rates were analyzed using one-way ANOVA. Data are presented as the mean ± SD; $*P < 0.05$, $**P < 0.001$. **(E)** Representative flow cytometry data for the MFI of human pSTAT3(705) in dMφs treated with a STAT3 inhibitor (NOR, INF, Stattic, and Stattic+INF groups). Representative data and the results of the statistical analysis of flow cytometry data for the frequency of LILRB4 expression in human **(F&G) or mouse (F&H)** dMφs treated with STAT3 inhibitors (NOR, INF, Stattic, and Stattic+INF groups, n = 6). The data are presented as the means ± SDs. P values of NOR versus INF and INF versus Stattic+INF were obtained via paired two-tailed Student's t tests. **(I)** Representative confocal images showing LILRB4 expression in human dMφ under the following conditions: NOR (uninfected), INF (infected), KLF6 siRAN926 alone, and KLF6 siRAN926+INF (n = 3). **(J&K)** Western blotting analysis of LILRB4 and KLF6 levels following transfection with three different KLF6 siRNAs (341, 831, 926) in *T. gondii*-infected human dMφ (n = 3); GAPDH served as an internal control.

Figure 4 *T. gondii* infection downregulates expression in dMφ via the pSTAT3(Y705)-KLF6 pathway

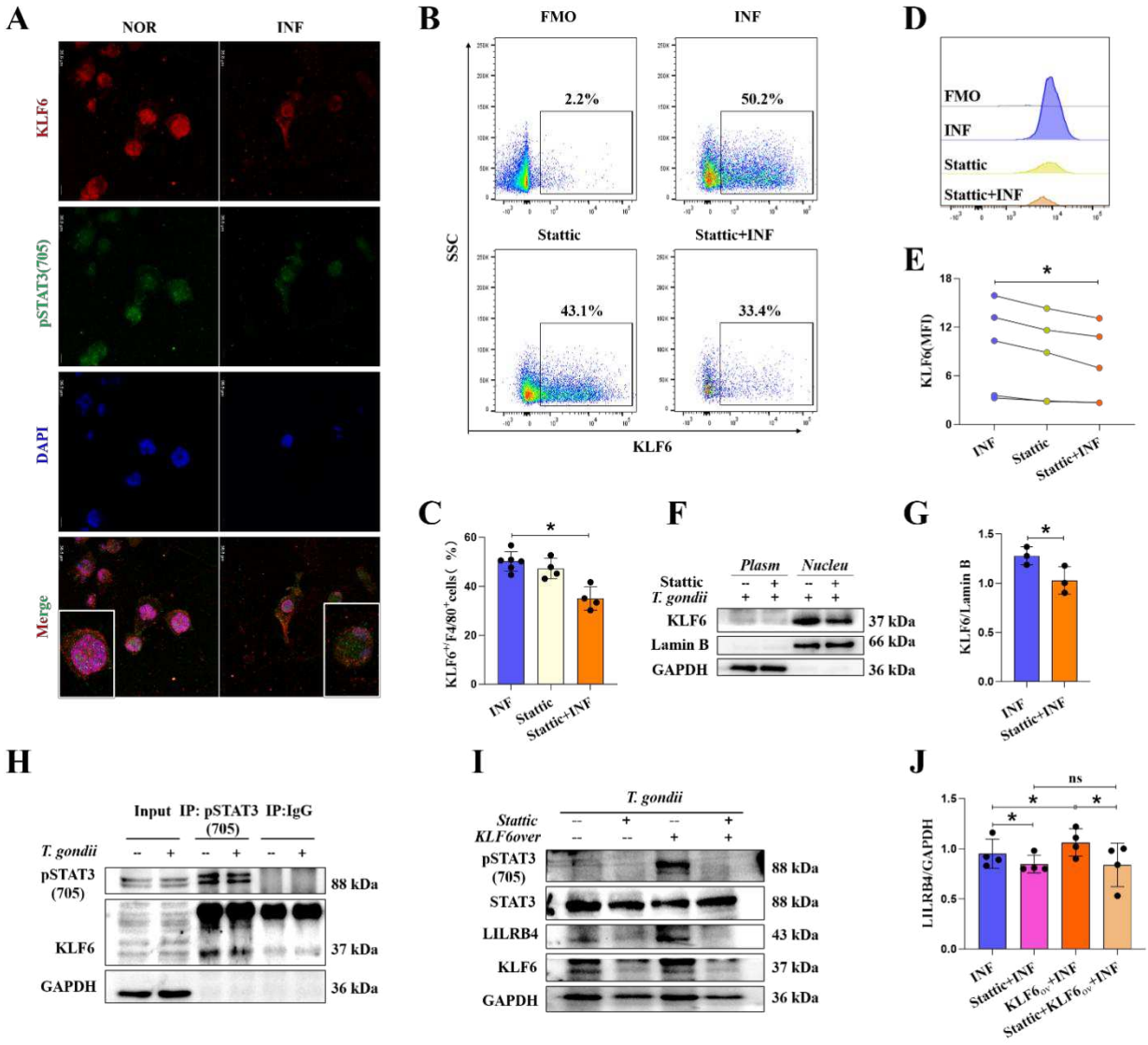

(A) Representative confocal images of pSTAT3 (705) and KLF6 in human dMφs from the NOR and INF groups (n >= 3). The data represent the mean ± SD. P values were obtained via paired one-tailed Student's t tests. NOR, normal human dMφ; INF, *T. gondii*-infected human dMφ. **(B&C)** Representative flow cytometry plots and quantitative analysis showing the frequency of $KLF6^+$ cells among mouse dMφ ($F4/80^+$) in the INF, Stattic, and Stattic+INF groups (n = 4–9). Data are presented as mean ± SD. *P*-values were determined using one-way ANOVA for comparisons between NOR *versus* INF and INF *versus* Stattic+INF. **(D&E)** Representative flow cytometry plots and statistical analysis of KLF6 mean fluorescence intensity (MFI) in

human dMφ ($CD14^+$) across the same treatment groups (n = 6). **(F&G)** Western blots and ImageJ-based quantification of pSTAT3 (Y705), KLF6, GAPDH, and Lamin B in cytoplasmic and nuclear extracts of human dMφ treated with a STAT3 inhibitor (INF, Stattic+INF; n = 3). GAPDH and Lamin B served as loading controls for cytoplasmic and nuclear fractions, respectively. Data are presented as mean ± SD. *P*-values were calculated using a paired two-tailed Student's t-test. **(H)** Coimmunoprecipitation (Co-IP) demonstrating the interaction between pSTAT3(Y705) and KLF6 in human dMφ with or without *T. gondii* infection. **(I&J)** Western blots and corresponding quantification of LILRB4, pSTAT3 (Y705), total STAT3, KLF6, and GAPDH of human dMφ treated with a STAT3 inhibitor or KLF6 overexpression (INF, Stattic+INF, $KLF6_{ov}$+INF, and Stattic+$KLF6_{ov}$+INF; n = 4). GAPDH was used as an internal control. Data are presented as the mean ± SD. *P*-values comparing NOR *versus* INF and INF *versus* Static+INF were calculated using a paired two-tailed Student's t-test.

Figure 5 LILRB4 downregulation inhibits the level of IDO in dMφ during *T. gondii* infection

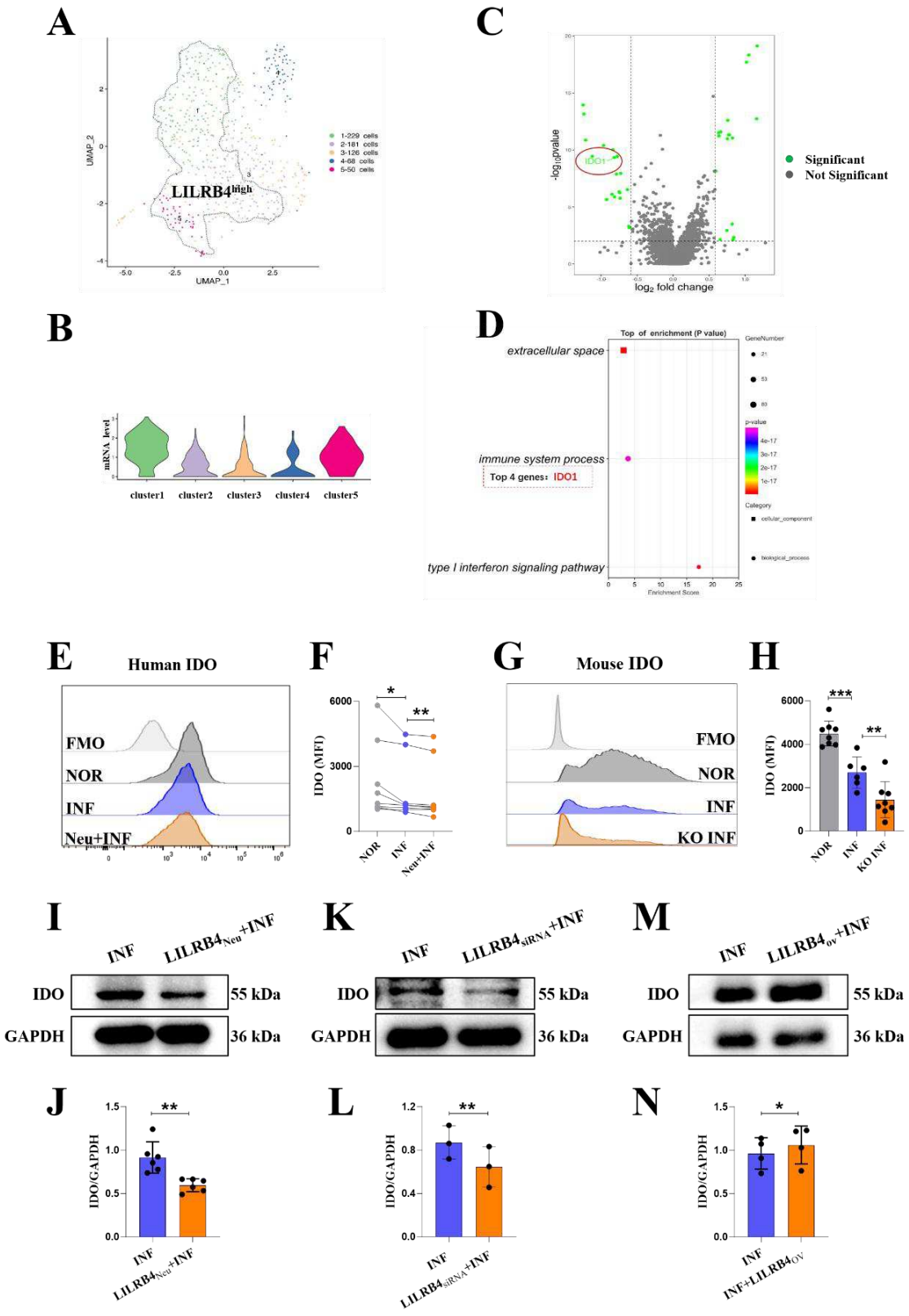

(A) The Uniform Manifold Approximation and Projection (UMAP) plot of 5 clusters

of human dMφ ($CD14^+$). (B) The expression profile of LILRB4 in 5 clusters of human dMφ. **(C) Volcano** plot of differentially expressed genes (DEGs) in LILRB4-high-expressing human dMφ with or without *T. gondii* infection. **(D)** Gene Ontology (GO) enrichment analysis showing the top three enriched biological processes among DEGs. **(E&F)** Representative flow cytometry plots and quantification of IDO mean fluorescence intensity (MFI) in human dMφ from NOR, INF, and LILRB4-neutralized INF groups (Neu+INF; n = 6). Data are represented as mean ± SD. *P*-values for NOR *versus* INF and INF *versus* Neu+INF were calculated using a paired two-tailed Student's t-test. **(G&H)** Flow cytometry plots and quantification of IDO MFI in mouse dMφ from NOR, INF, and LILRB4 knockout (KO) + INF groups (n = 6 – 8). *P*-values were determined by one-way ANOVA. Western blotting analysis and ImageJ-based quantification of IDO and GAPDH expression in human dMφ treated with a LILRB4-neutralizing antibody (INF, Neu+INF; n = 9) **(I&J)**, LILRB4 siRNA **(K&L)** ($LILRB4_{siRNA}$+INF; n = 3), and LILRB4 overexpression plasmid ($LILRB4_{ov}$+INF; n = 4) **(M&N)** during *T. gondii* infection. GAPDH was used as the loading control. Data are shown as mean ± SD. *P*-values were calculated using a paired two-tailed Student's t-test.

Figure 6 LILRB4 downregulation mediated the reduction of IDO by inhibiting the SHP-1 pathway during *T. gondii* infection

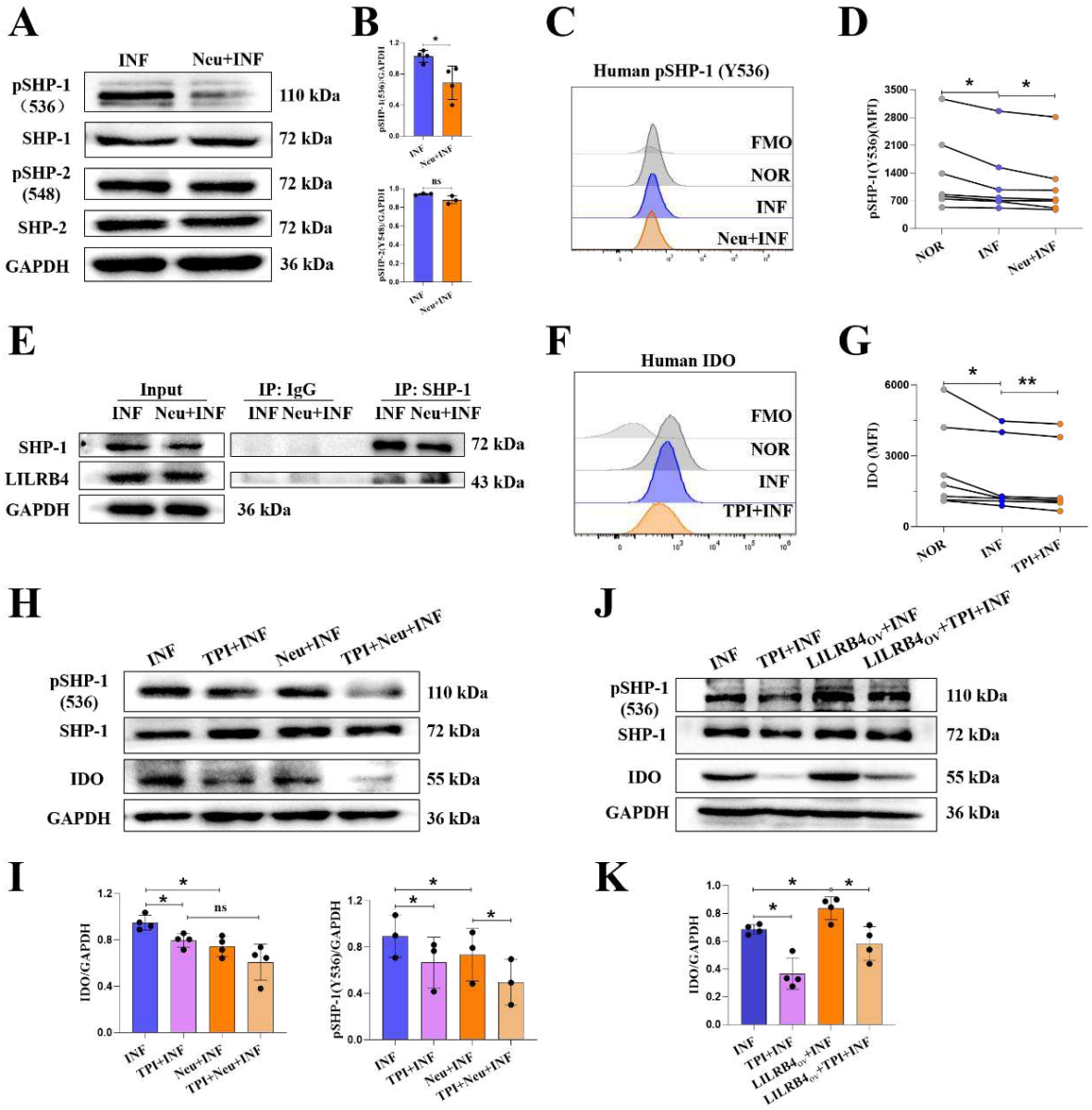

(A & B) Western blot analysis and quantification by Image J of pSHP-1 (Y536), SHP-1, pSHP-2 (Y548), SHP-2, and GAPDH of human dMφ treated with a LILRB4-neutralizing antibody (INF and Neu+INF). n = 3 – 4) during *T. gondii* infection. GAPDH was regarded as the internal reference. The data are represented as mean ± SD. P-value was obtained by paired two-tailed Student's t-test. **(C & D)** Representative data and their statistical analysis of flow cytometry for the MFI of pSHP-1(Y536) in human dMφ of the NOR, INF, and LILRB4-neutralized plus INF

groups (n = 6). The data are represented as mean ± SD. *P*-values of NOR *versus* INF and INF *versus* Neu+INF were obtained by paired two-tailed Student's t-tests. **(E)** Co-IP analysis of the interaction between SHP-1 and LILRB4 in human dMφ of the INF and LILRB4-neutralized plus INF groups (n = 3). **(F&G)** Representative data and their statistical analysis of flow cytometry for the MFI of IDO in human dMφ of the NOR, INF, and SHP-1 inhibitor plus INF groups (n = 6). The data are represented as mean ± SD. *P*-values of NOR versus INF and INF *versus* TPI+INF were obtained by paired two-tailed Student's t-tests. **(H&I)** Western blot analysis and quantification by Image J of pSHP-1(Y536), SHP-1, IDO, and GAPDH of human dMφ treated with a LILRB4-neutralizing antibody or a SHP-1 inhibitor (INF, TPI+INF, Neu+INF, and TPI+Neu+INF; n = 3 – 4) during *T. gondii* infection. GAPDH was regarded as the internal reference. The data are represented as mean ± SD. The P-value is obtained by a paired two-tailed Student's t-test with INF *versus* TPI+INF, INF *versus* Neu+INF, TPI+INF versus TPI+Neu+INF, and Neu+INF *versus* TPI+Neu+INF. **(J&K)** Western blot analysis and quantification by Image J of pSHP-1(Y536), SHP-1, IDO, and GAPDH of human dMφ treated with a LILRB4 overexpression plasmid or a SHP-1 inhibitor (INF, TPI+INF, $LILRB4_{ov}$+INF, and $LILRB4_{ov}$ +TPI+INF; n= 3-4) during *T. gondii* infection. GAPDH was regarded as an internal reference. The data are represented as mean ± SD. *P*-value was obtained by paired two-tailed Student's t-test with INF *versus* TPI+INF. INF *versus* $LILRB4_{ov}$ + INF, TPI+INF *versus* LILRB4ov + TPI+INF, $LILRB4_{ov}$ + INF *versus* $LILRB4_{ov}$ + TPI+INF.

Figure 7 LILRB4 downregulation undermines macrophage function by inhibiting IDO via the SHP-1/JAK2/STAT1 signaling axis during infection

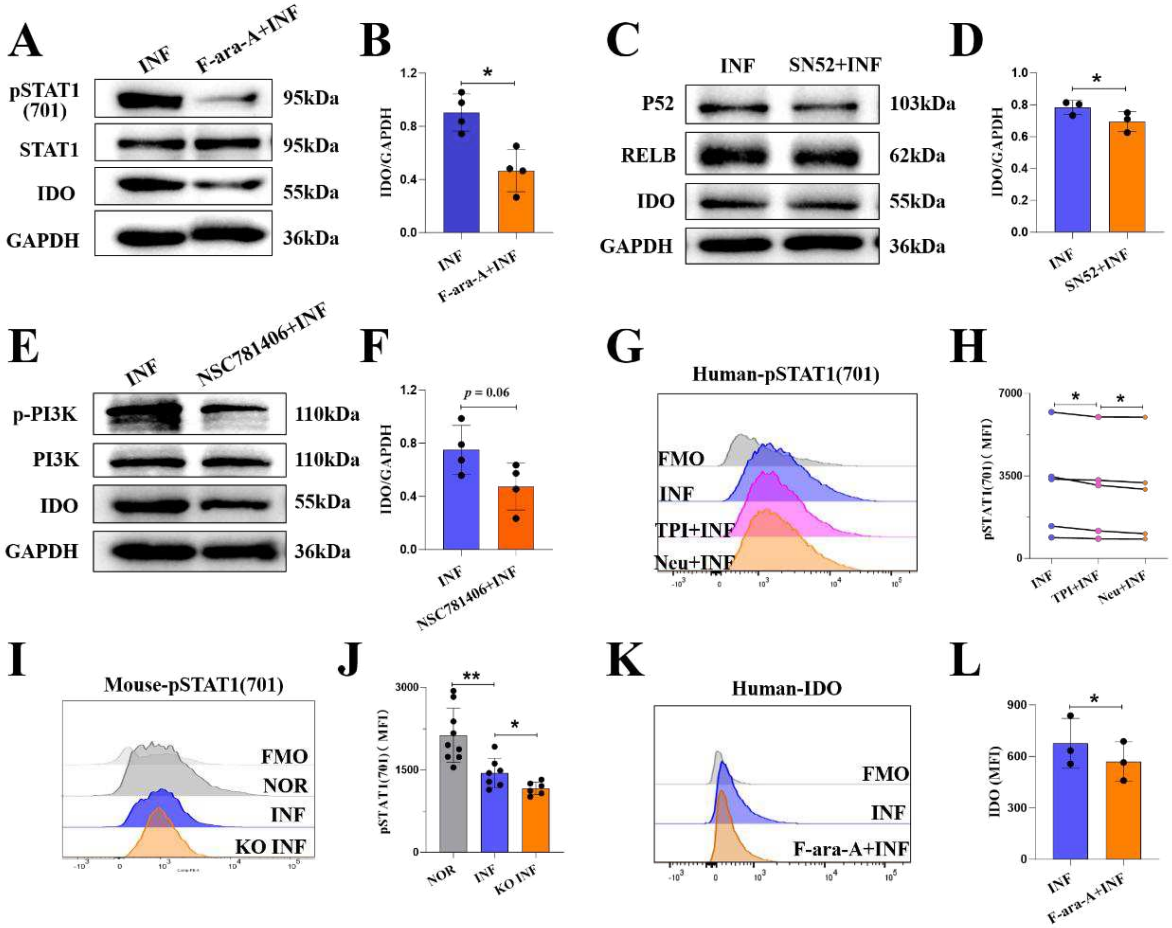

(A and B) Western blot analysis and quantification by Image J of pSTAT1 (701), STAT1, IDO, and GAPDH of human dMφ treated with the STAT1 inhibitor (F-ara-A; n = 4) during *T. gondii* infection. GAPDH was regarded as an internal reference. **(C & D)** Western blot analysis and quantification by Image J of P52, RelB, IDO, and GAPDH of human dMφ treated with a P52 inhibitor (INF, P52in+INF). n = 3) during *T. gondii* infection. **(E&F)** Western blot analysis and quantification by Image J of pPi3k, Pi3k, IDO, and GAPDH of human dMφ treated with a PI3K inhibitor (INF, PI3kin+INF; n = 4) during *T. gondii* infection. GAPDH was regarded as the internal reference. The data are represented as mean ± SD. The P-value is obtained by a paired two-tailed Student's t-test with INF versus Pi3kin+. **(G&H)** Representative data and their statistical analysis of flow cytometry for the MFI of pSTAT1(701) in LILRB4-neutralized and SHP-1 inhibitor (TPI)-treated human dMφ during *T. gondii* infection (INF, Neu+INF, and TPI+INF; n= 5). The data are represented as mean ± SD. *P*-

values were obtained by paired two-tailed Student's t-tests with INF *versus* Neu+INF and INF *versus* TPI+INF. **(I&J)** Representative data and their statistical analysis of flow cytometry for the MFI of pSTAT1(701) in LILRB4 knockout (KO) mouse dMφ during *T. gondii* infection (NOR, INF, and KO+INF; n= 7-9). The data are represented as mean ± SD. *P*-values were obtained by unpaired two-tailed Student's t-test with NOR *versus* INF and INF *versus* KO+INF. **(K&L)** Representative data and their statistical analysis of flow cytometry for the MFI of IDO in STAT1 inhibitor-treated human dMφ during *T. gondii* infection (INF and F-ara-A+INF; n= 3).

Figure 8 LILRB4 downregulation compromises macrophage function by suppressing IDO expression via the SHP-1/JAK2/STAT1/IRF1 pathway during *T. gondii* infection

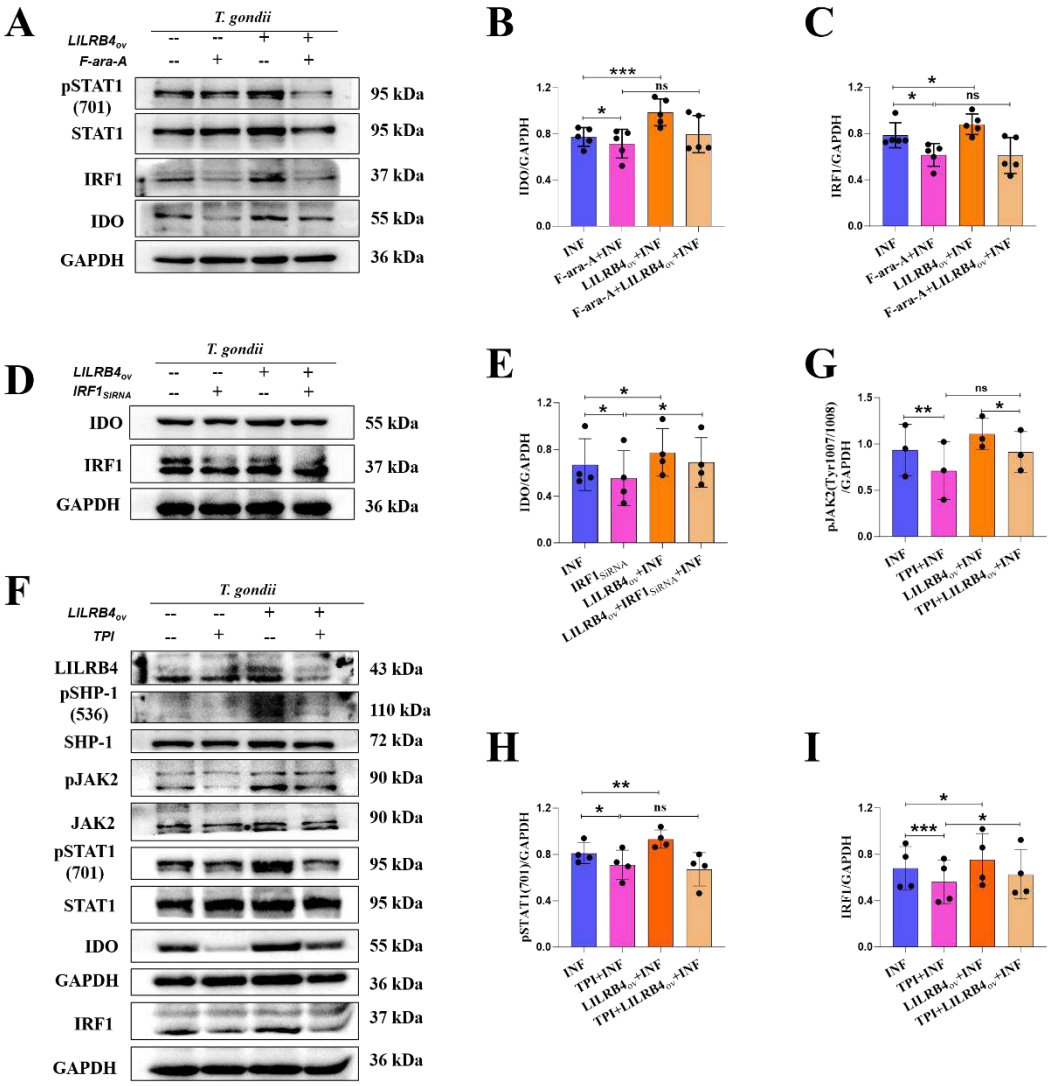

(A-C) Western blot analysis and quantification by Image J of IRF1, pSTAT1 (701), STAT1, IDO, and GAPDH of human dMφ treated with the STAT1 inhibitor (F-ara-A) and the LILRB4 overexpressed plasmid (INF, F-ara-A+INF, LILRB4ov+INF, and F-ara-A+LILRB4ov+INF). n = 5) during *T. gondii* infection. GAPDH was regarded as the internal reference. The data are represented as mean ± SD. *P*-values were obtained by paired two-tailed Student's t-tests with INF *versus* F-ara-A +INF, INF *versus* LILRB4$_{ov}$+INF, F-ara-A +INF *versus* F-ara-A +LILRB4ov+INF, and LILRB4$_{ov}$+INF *versus* F-ara-A +LILRB4$_{ov}$+INF. **(D & E)** Western blot analysis and quantification

by Image J of IRF1, IDO, and GAPDH of human dMφ treated with IRF1 siRNA and LILRB4 overexpression plasmid (INF, IRF1siRNA + INF, LILRB4ov + INF, and $IRF1_{siRNA}$ + LILRB4ov + INF). n = 4) during *T. gondii* infection. GAPDH was regarded as the internal reference. The data are represented as mean ± SD. *P*-values were obtained by paired two-tailed Student's t-tests with INF *versus* $IRF1_{siRNA}$+INF, INF *versus* $LILRB4_{ov}$+INF, $IRF1_{siRNA}$+INF *versus* $IRF1_{siRNA}$ +LILRB4ov+INF, and $LILRB4_{ov}$+INF *versus* $IRF1_{siRNA}$ +$LILRB4_{ov}$+INF. **(F-I)** Western blot analysis and quantification by Image J of pSHP-1(Y536), SHP-1, LILRB4, pJAK2(Tyr1007/1008), JAK2, IRF1, pSTAT1(701), STAT1, IDO, and GAPDH of human dMφ treated with a SHP-1 inhibitor and LILRB4 overexpressed plasmid (INF, TPI+INF, LILRB4ov+INF, and TPI+LILRB4ov+INF). n = 3-5) during *T. gondii* infection. GAPDH was regarded as the internal reference. The data are represented as mean ± SD. *P*-values were obtained by paired two-tailed Student's t-tests with INF *versus* TPI+INF, INF *versus* $LILRB4_{ov}$+INF, TPI+INF *versus* TPI+LILRB4ov+INF, and $LILRB4_{ov}$+INF *versus* TPI+$LILRB4_{ov}$+INF.

Figure 9 LILRB4 downregulation impairs macrophage function by upregulating iNOS expression via the SHP-1/PI3K/c-Fos pathway during *T. gondii* infection

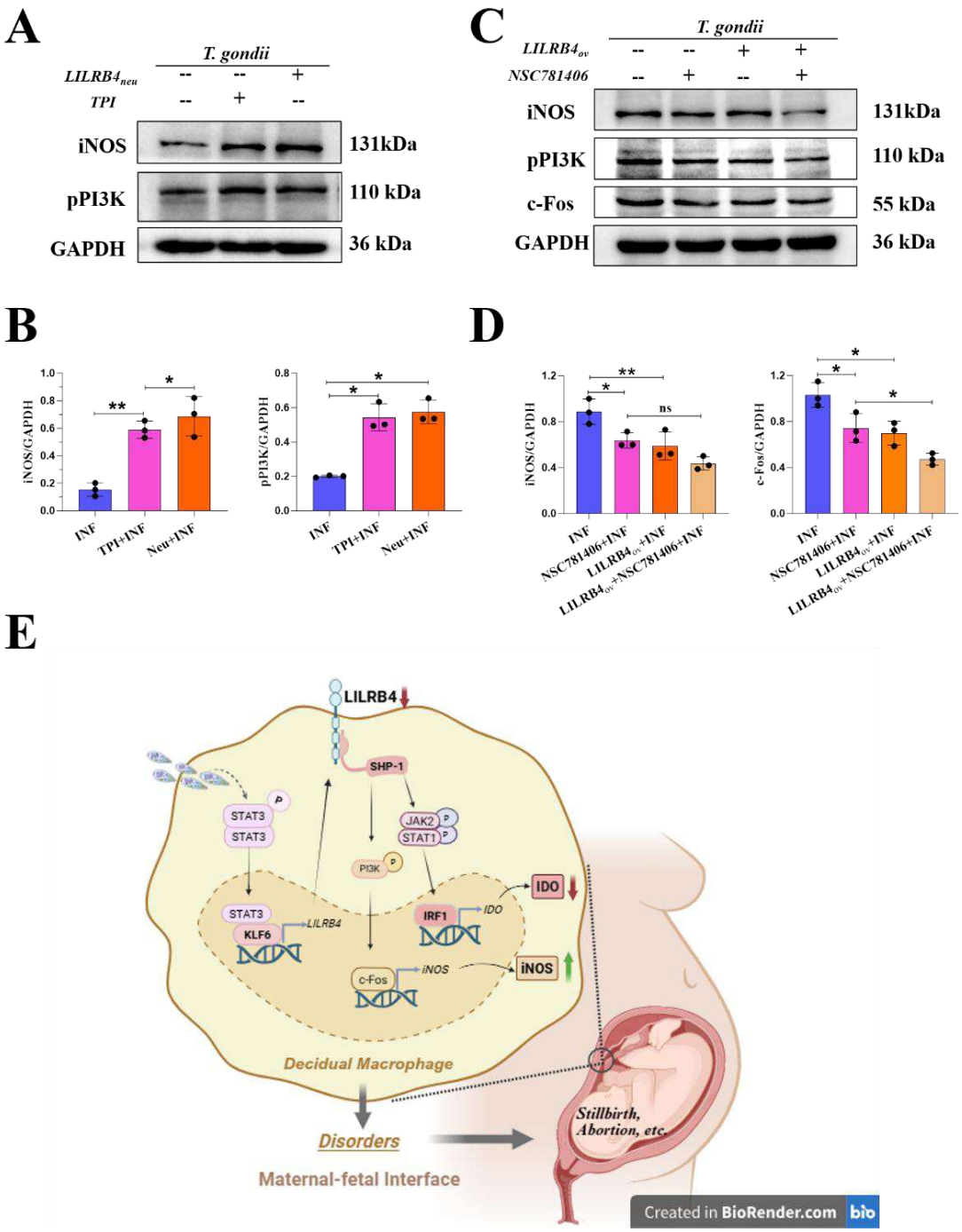

(**A & B**) Western blot analysis and quantification by Image J of iNOS and pPI3K, and GAPDH of human dMφ treated with a SHP-1 inhibitor and a LILRB4 neutralizing antibody (INF, TPI+INF, LILRB4neu+INF; n = 4) during *T. gondii* infection. GAPDH was regarded as the internal reference. The data are represented as mean ± SD. *P*-

values were obtained by paired two-tailed Student's t-tests with INF *versus* TPI+INF, INF *versus* LILRB4$_{neu}$+INF. (**C & D**) Western blot analysis and quantification by Image J of iNOS, pPI3K, c-Fos, and GAPDH of human dMφ treated with a PI3K inhibitor (NSC781406) and a LILRB4 overexpression plasmid (INF, NSC781406+INF, LILRB4ov+INF, and NSC781406+LILRB4$_{ov}$+INF. n = 3) during *T. gondii* infection. GAPDH was regarded as the internal reference. The data are represented as mean ± SD. *P*-values were obtained by paired two-tailed Student's t-tests with INF *versus* NSC781406+INF, INF *versus* LILRB4$_{ov}$+INF, NSC781406+INF *versus* NSC781406+LILRB4ov+INF. **(E)** This study elucidates that *T. gondii* infection downregulates the expression of LILRB4 on dMφ by suppressing the transcription factor KLF6 and impairing its binding to the LILRB4 promoter. This process is mediated through the inhibition of STAT3 phosphorylation. The downregulation of LILRB4 disrupts the immunoregulatory balance of dMφ, characterized by a significant decrease in IDO and an increase in iNOS expression. Mechanistically, LILRB4 deficiency attenuates IDO via the pSHP-1/pJAK2/pSTAT1(701)/IRF1 pathway, while promoting iNOS expression through the pSHP-1/pPI3K/c-Fos signaling axis.

TABLE 1 The sequence information of potential binding sites of transcription factor KLF6 with the upstream promoter of LILRB4

Matrix ID	Name	Score	Start	End	Predicated Sequence
MA1517.1	MA1517.1. KLF6	15.32	591	601	CACCACGCCCA
MA1517.1	MA1517.1. KLF6	13.53	1967	1977	GGCCACACCCT
MA1517.1	MA1517.1. KLF6	6.50	641	651	TGATCCGCCCA
MA1517.1	MA1517.1. KLF6	6.17	181	191	CCTCCCACCCT
MA1517.1	MA1517.1. KLF6	5.75	822	832	GATCACACCAC
MA1517.1	MA1517.1. KLF6	5.15	2041	2051	GGAGACGCCAT
MA1517.1	MA1517.1. KLF6	4.88	1194	1204	GCCCAGACCCT
MA1517.1	MA1517.1. KLF6	4.76	1002	1012	GGACCTGCCCA
MA1517.1	MA1517.1. KLF6	4.63	1288	1298	CATCAGGCCCA
MA1517.1	MA1517.1. KLF6	4.51	297	307	GGGCACGTCCT

Legends To Supplementary Figures

Supp. Figure 1 The gating strategy of flow cytometry of dMφ

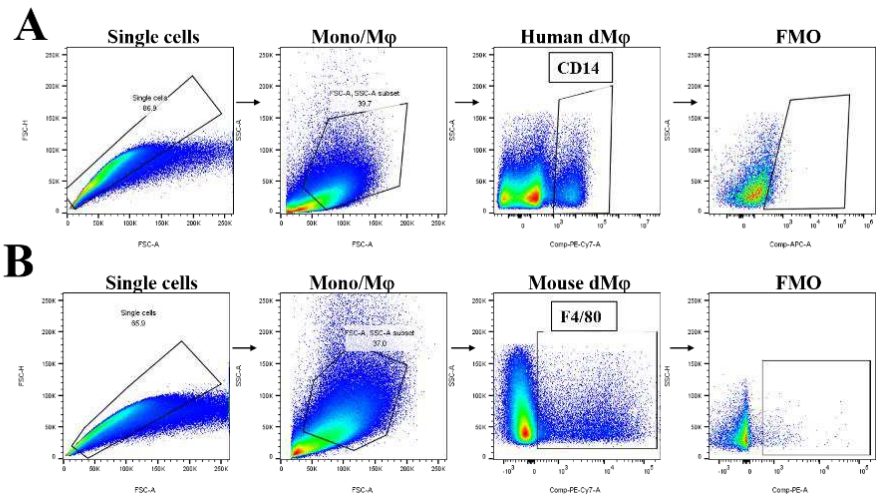

The gating strategy of flow cytometry of human **(A)** or mouse **(B)** dMφ in this study. Fluorescence Minus One control (FMO), the control.

Supp. Figure 2 The effect of KLF6 knockdown on LILRB4 expression in dMφ during *T. gondii* infection.

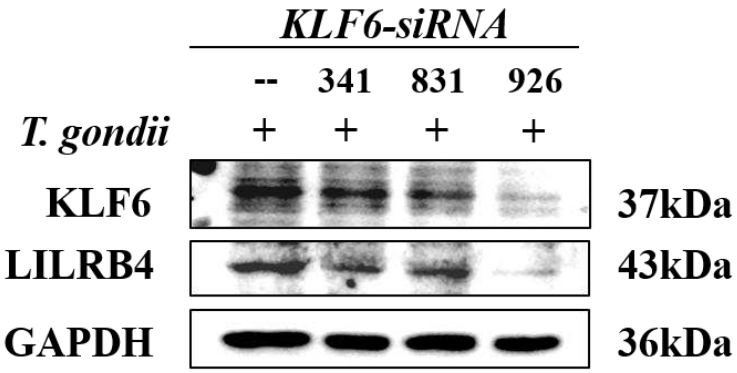

Western blot analysis of LILRB4 of human dMφ treated with three different KLF6 siRNAs (INF, $KLF6_{siRNA\text{-}341}$+INF, $KLF6_{siRNA\text{-}831}$+INF, $KLF6_{siRNA\text{-}926}$+INF) during *T. gondii* infection. GAPDH was regarded as an internal reference.

Supp. Figure 3 The effect of LILRB4 knockdown on IDO expression in dMφ during *T. gondii* infection

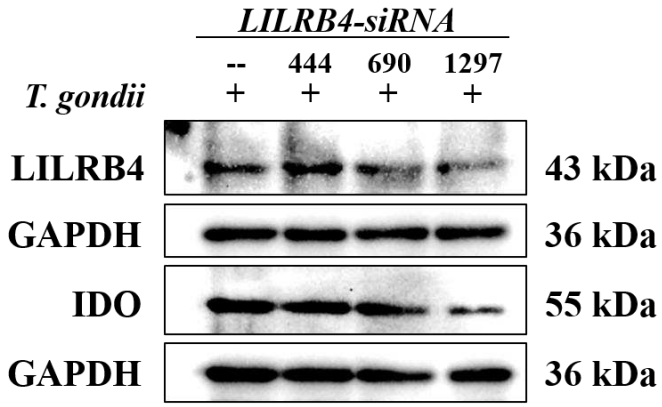

Western blot analysis of IDO of human dMφ treated with three different LILRB4 siRNAs (INF, LILRB4$_{siRNA-1}$+INF, LILRB4$_{siRNA-2}$+INF, LILRB4$_{siRNA-3}$+INF) during *T. gondii* infection. GAPDH was regarded as an internal reference.

Supp. Figure 4 The effect of IRF1 on IDO expression in dMφ during *T. gondii* infection

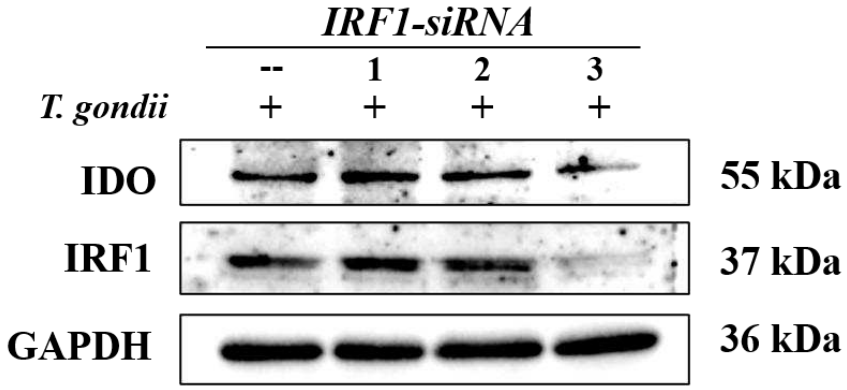

Western blot analysis of IDO of human dMφ treated with three different IRF1 siRNAs (INF, IRF1$_{siRNA-1}$+INF, IRF1siRNA-2+INF, IRF1$_{siRNA-3}$+INF) during *T. gondii* infection. GAPDH was regarded as an internal reference.